



# Resistivity method contribution in determining of fault zone and hydro-geophysical characteristics of carbonate aquifer, eastern desert, Egypt

A. I. Ammar<sup>1</sup> · K. A. Kamal<sup>1</sup>

Received: 6 July 2014 / Accepted: 31 August 2017 / Published online: 8 January 2018  
© The Author(s) 2018. This article is an open access publication

## Abstract

Determination of fault zone and hydro-geophysical characteristics of the fractured aquifers are complicated, because their fractures are controlled by different factors. Therefore, 60 VESs were carried out as well as 17 productive wells for determining the locations of the fault zones and the characteristics of the carbonate aquifer at the eastern desert, Egypt. The general curve type of the recorded rock units was QKH. These curves were used in delineating the zones of faults according to the application of the new assumptions. The main aquifer was included at end of the K-curve type and front of the H-curve type. The subsurface layers classified into seven different geoelectric layers. The fractured shaly limestone and fractured limestone layers were the main aquifer and their resistivity changed from low to medium (11–93 Ω m). The hydro-geophysical properties of this aquifer such as the areas of very high, high, and intermediate fracture densities of high groundwater accumulations, salinity, shale content, porosity distribution, and recharging and flowing of groundwater were determined. The statistical analysis appeared that depending of aquifer resistivity on the water salinities (T.D.S.) and water resistivities add to the fracture density and shale content. The T.D.S. increasing were controlled by Na<sup>+</sup>, Cl<sup>-</sup>, Ca<sup>2+</sup>, Mg<sup>2+</sup>, and then (SO<sub>4</sub>)<sup>2-</sup>, respectively. The porosity was calculated and its average value was 19%. The hydrochemical analysis of groundwater appeared that its type was brackish and the arrangements of cation concentrations were Na<sup>+</sup> > Ca<sup>2+</sup> > Mg<sup>2+</sup> > K<sup>+</sup> and anion concentrations were Cl<sup>-</sup> > (SO<sub>4</sub>)<sup>2-</sup> > HCO<sub>3</sub><sup>-</sup> > CO<sub>3</sub><sup>-</sup>. The groundwater was characterized by sodium–bicarbonate and sodium–sulfate genetic water types and meteoric in origin. Hence, it can use the DC-resistivity method in delineating the fault zone and determining the hydro-geophysical characteristics of the fractured aquifer with taking into account the quality of measurements and interpretation.

**Keywords** DC-resistivity method · VESs · Fault zones · Hydro-geophysical characteristics · Statistical analysis · Hydrochemical analysis · Carbonate aquifer

## Introduction

In general, groundwater is the major source to supply the water needed for industrial, agricultural, and domestic purposes and hence largely contribute to the economic development of such regions, especially for those exposed to arid and semi-arid climatic conditions, where the surface water resource is limited. The increasing stress on groundwater exploitation in such areas causes decline in its level

consequently confining the flow to fractured zones of aquifer and thus making the situation alarming. Cemen et al. (2008) and Halihan (2008) reported that the fractures in aquifer rocks affect the flow of water, and therefore, numerical modeling of the fluid flow requires an understanding of the geometry and density of fractures that have a great influence on the discharge and recharge mechanisms. The lack of characterization data generally comes from the cost involved in drilling, completing, maintaining, and sampling wells. This cost is higher in fracture and karstic aquifers due to the higher drilling costs and the heterogeneous flow fields typically require more data than are available from discrete sampling techniques which provide only limited two- or three-dimensional data. Most of methods of characterizing these aquifers have relied on two detection and monitoring

✉ A. I. Ammar  
abdallah\_ammam\_708@hotmail.com

<sup>1</sup> Research Institute for Groundwater, National Water Research Center, Cairo, Egypt

strategies. The first strategy involves discrete point sampling of fluids using wells, springs, or multilevel piezometers for integration and interpretation. The second strategy uses indirect measurements through surface or bore-hole geophysical techniques. Therefore, at this study for understanding this complex fractured aquifer and for giving the facilities for studying and for solution the complex determinations of the different hydrogeological parameters of this aquifer, we used the surface resistivity method which depended on the impedance of the electrical current during penetration through the subsurface conductive and non-conductive rocks, to provide more complete site data coverage, with the available hydrogeological data. In general, flow features (such as faults that conduct fluids) and higher porosity lithologies are indicated by low-resistivity anomalies. In addition, the hydraulic parameters of the formation may be estimated using electrical methods (Purvance and Andricevic 2000a, b). The electrical data produced from this type of study may help characterize heterogeneity, fractures, and aquifer parameters (Herwanger et al. 2004; Niwas and de Lima 2003). Carbonate aquifers are complex in nature and are subjected to high variability of the hydrogeological parameters depending on the fractures distribution and interconnect between them. The carbonate aquifers are normally traversed by lineaments such as fault and fracture zone distributions that make the groundwater dynamics more complex, and hence, their characteristics become more important to understand the fractured aquifer setup. These fault and fracture zones play an important role in the groundwater dynamics and it act as indicator to locate the groundwater resources and also the expected feeding of the aquifer either from the deep aquifer, from the neighborhood aquifer, or from streams. In general, the waids or drainage patterns over the hard rocks are controlled by the subsurface structure-like faults. These drainages are interesting in feeding the subsurface aquifer and the water into the fractures will be mixed water if the faults assisted in connecting with the deep aquifer. Therefore, these features are very important in expecting the potentialities of the subsurface aquifer with focusing on the horizontal and vertical conductive fracture zone distributions and the down-throw or up-throw of the recorded faults and may be the potentialities increased far away from the faults, or fault should be avoided or there is really nothing linear available in area, where it is needed. Hence, there is need of detailed characterization of lineaments and its validation for the groundwater potentiality and feeding.

Chandra et al. (2006) have demonstrated that the geophysical characterization helps in understanding about the expected potentialities of the hard rocks. Accordingly, at this study, the surface data from resistivity method and geomorphological data and subsurface data, geological and hydrogeological data, from boreholes, and hydrochemistry data were used in understanding the expected geophysical,

geological, and hydrogeological properties of the carbonate aquifer. These data assisted in how to delineate the faults, fracture zone distribution, distribution of shale horizontally and vertically, groundwater quality, the role of faults in connection between multiple aquifers, and the expected source of groundwater. According to geoelectrical and hydrochemical, geological, and hydrogeological properties of this aquifer, it is assumed that the fractures density and intensity of the carbonate aquifer distributed horizontally and vertically and may control by structure tectonics such as faults. These features may important in feeding this aquifer and controlling in its groundwater quality adds to determine the locations of low and high groundwater accumulation. Therefore, geophysical methods are occasionally used to characterize karstic features (caves, sinkholes, faults, and fractures) prior to any hydrogeological or geological studies.

In general, the electric conduction in most rocks is essentially electrolytic. This is because most mineral grains, except metallic ores and clay minerals, are insulators, electric conduction being through interstitial water in pores and fissures or fractures. Groundwater filling the pore space of a rock is a natural electrolyte with a considerable amount of ions present to add to conductivity. As a rule, the more porous or fissured/fractured a rock and the larger its groundwater content, the higher is the conductivity and the lower is the resistivity. If clay minerals are present in a water-bearing rock, a relatively large number of ions may be released from such minerals by ion-exchange processes, the ions contributed by these processes add to the normal ion concentration in pore water, and the net result being an increasing conductivity. All rocks containing clay minerals (in wet state) exhibit abnormally high conductivity in this account. Hard rocks are bad conductors of electricity, but many geological processes can alter a rock and significantly lower its resistivity. For instance, dissolution, faulting, shearing, columnar jointing, weathering, and hydrothermal alteration usually increase the rock porosity and fluid permeability, and hence lower resistivity. At this study, it is believed that the dissolution in the form of small caves or vugs and faulting in form of fractures, fissures, and joints. These processes are more abundant in the areas of low resistivities values which reflect the very high-to-high fractures. In contrast to the above processes, precipitation of calcium carbonate ( $\text{CaCO}_3$ ) or silica reduces porosity and hence increases resistivity. These processes are more appearance in the areas of high-resistivity values which reflect the presence of intermediate fractures with respect to the occurring of major caves which may be resulted from the replacement of calcium sulfate ( $\text{CaSO}_4$ ) (Sharma 1997).

### Study area setting

In general, the aquifer under study covers vast areas in Egypt (Fig. 1) and it extended to neighbored countries to the north of Africa and may complicate and change from area to other. The chosen area for studying this aquifer is located at the eastern desert of Egypt to the east of Beni-Suef governorate, specifying in the east of El-Fashn town between longitudes 30°54'36" and 31°04'12"E, and latitudes 28°47'24" and 28°52'12"N (Fig. 1).

This area located on the limestone plateau (Middle Eocene) characterizes with several topographic features. These features include hills, plateaus, mountains, and dry wadis (streams). It was believed that these streams and their tributaries generated from the rainfall or from the structure controlling and may consider the main source in recharging the subsurface aquifer in several areas. Wadi El-Faqira is the main wadi at the study area and its general direction is from southeast, where the plateau, to northwest, where the Nile valley (Fig. 1). The climate of this area is arid, with occasional rainfall mainly in March (high rate). The winter diurnal temperature range is 7–21 °C (from November to February), in the summer from July to August, and temperature reaches daytime maximum of more than 37 °C (ranged from 22 to 37 °C).

### Geology

Good knowledge of the lithology, stratigraphy, and structures reveals a better understanding of the hydrogeological conditions of groundwater occurrences, comprising the flow patterns, electrical, and other hydrogeological characteristics at any subsurface media. Moreover, the geologic setting displays one of the important elements which form and control the hydrogeologic regime of any area. This topic was illustrated more details by Abd El-Mageed (2002).

The lithostratigraphic sequence of the surface succession is formed of the sedimentary rock units which belong to Upper and Middle Eocene and Pliocene of Tertiary ages and Quaternary ages. The Upper and Middle Eocene are formed of limestone, marls, clays, and shales. The Pliocene is formed of conglomerates and sandstone, while the quaternary is formed of sands, gravel, sand, and silt. All these units were exposed, but nearly, nowhere, the complete succession is recorded. The lithologic facies and their thicknesses vary either laterally or vertically. Data were compiled from the surface outcrops during visiting the authors to the area for carrying out the geophysical surveying and during supervising on the drilling of 17 wells. A composite lithostratigraphic sequence of the exposed rock units in Beni-Suef area is compiled in the present study (Table 1). It has a thickness of +442 m. The nomenclatures of the rock unit as proposed by the previous authors are followed. The exposed rock units are discussed as follows from base to top.

The Eocene rock units have a wide distribution and are mainly represented by extension of Middle Eocene rocks.

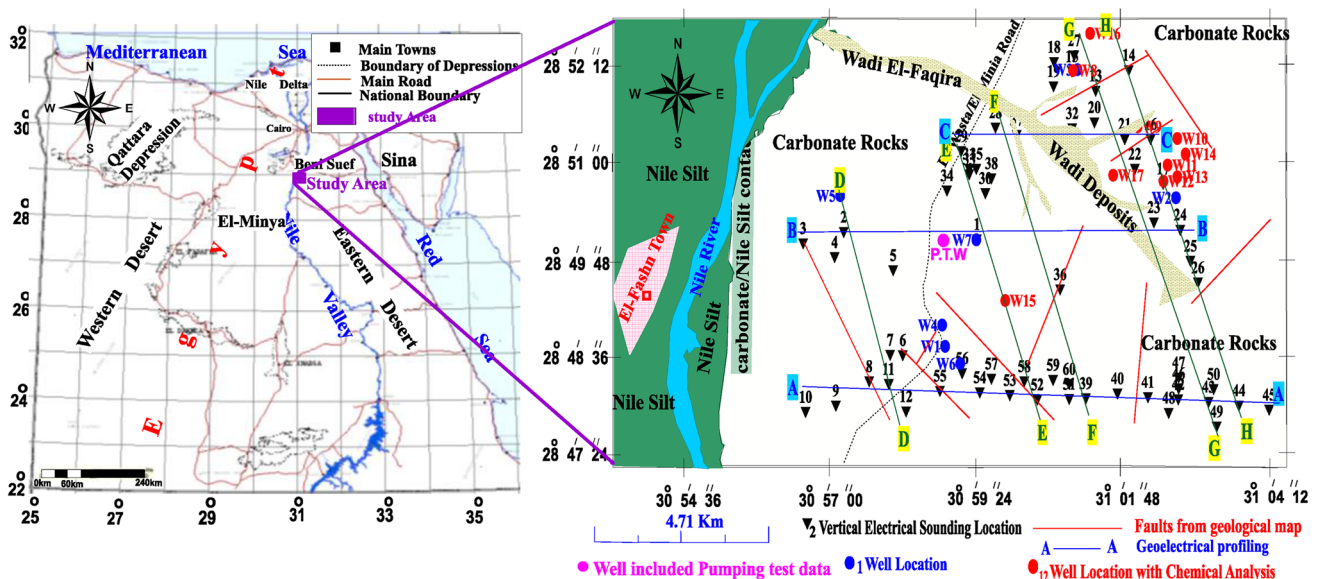


Fig. 1 General location map of the study area (small shadow quadrangle) (left), and distribution map of VESs, well locations, and geoelectrical profiles (right)

**Table 1** Composite lithostratigraphic section of the exposed rock units, Beni-Suef area, Egypt (Modified after, Abd El-Mageed 2002)

Age		Formation	Member	Symbol	Max. thick	Lithologic discription	Occurence			
Quaternary	Holocene	Sand Duns			Variable	Sands	Cultivated land in the Nile Valley			
		Nile Silt			15m	Silt and clay				
	Pleistocene	Abbassia Fm.			Variable	Gravel, sands and clays	Nile Valley area			
		Sath Ghorab Fm.			Variable	Sandstone				
		Kasr El-Basel Fm.			25m	Gravel, sands and S.stone				
Tertiary	Pliocene	Um Raqaba Fm.	Divided into Qurn Member, Tarbul Member, Observatory Member		40 m	Conglomerates and Sandstone	G. (Umm Raqabs, Labum, El-Naalun)			
		Eocene			U. Eocene	Maadi Fm.	30 m	Impure sand coquinooid L.S, marl and clay toppest with crystalline L.S	G.Homret Shaibun	
	Middle					Lower Mokattam Fm.	Upper Mokattam	62 m	Nodular Limestone Nummulitic and marl with minor clay interbeds	Gebel Homret Shaibun north east of Beni-Suef
					Eocene		Beni-Suef Fm.	100 m	Argillaces Limestone top laminated clays, Argillaces Limestone interbeded with clay and calcareous clay	Exposures lying south east of Beni-Suef and G. Shaibun
							El-Fashn Fm.	90 m	Different facies north: limestone and marl complex south: chalky limestone and gypsiferous shales with chert	Exposures east of Beni-Suef
	Eocene				Lower Mokattam Fm.	Qarara Fm.	80 m	Karstified Nummulitic Limestone and (with caves)	East of Beni-Suef in G. Sannur and G. Ghayda west of Beni-Suef G. Qarara	
						Pre Middle Eocene not exposed		Total thickness = 442 m		

They are recognized in the Eastern and Western Plateaux as well as in the subsurface of the Nile Valley. While the Upper Eocene rocks were reported in Gebel Homeret Shaibun lying east and Gebel El-Naalun lying west of the Nile Valley. The sequence of the Middle Eocene is formed of four rock units from base to top as follows: Qarara Formation, EL-Fashn Formation, Beni-Suef Formation, and Shaibun Member, while the Upper Eocene sequence is represented of one rock unit (Maadi Formation). It has to be mentioned that the Upper Eocene is very coordinate in the study area (Table 1). The Eocene rock units at Beni-Suef area are summarized from base to top as follows, according to Abd El-Mageed (2002) description:

- (a) Qarara Formation (Middle Eocene): the term Qarara Formation was introduced for the Middle Eocene sequence (Upper Lutetian age) east of Maghagha at G. Qarara. It has a thickness of 170 m and is composed of shale, marl, sandstone, and sandy limestone. West of Beni-Suef area, the exposed section of Qarara Formation has a thickness of 80 m. The Qarara Formation at Beni-Suef area is characterized by fractures, partings veins, veinlets, and geodes filled with calcite. Subsurface caves were developed along the intersection of fractures (Karstified Limestone). Surface quarries were dug that reached the depth of caves (Abd El-Mageed 2002).

(b) El-Fashn Formation (Middle Eocene): it was defined in most of the exposed section lying east and west of Beni-Suef area. Its maximum thickness is 90 m and exposed at G. Muhami and wadi El Shaikh east of Beba and at Warshat El-Rukham, G. Umm Raqaba, and G. Mashash lying south east of Beni-Suef. All these places were recorded in Table 1 with focusing on the famous names to the east at the study area. It is distinguished by different facies, since it is built up of chalky limestone with chert bands or nodules followed upward by green shales with gypsum vienlets at wadi El Sheikh. It changes northward into grayish green and gypsiferous at Warshat El-Rukham (the marble factory). Furthermore, its facies change into marly limestone interbedded with shale at G. E1 Mashash and into limestone and marl sequence at G. Shaibun (Table 1).

The quaternary rock units: the Pleistocene and Holocene deposits in the Nile Valley particularly in Upper Egypt are dealt by innumerable. The Nile trough possesses the more complete record of the quaternary in Egypt, where the sediments assume great thicknesses. These quaternary deposits unconformable overlie generally the Middle Eocene rocks and underlie unconformable the Holocene sediments. The Pleistocene deposits attain a thickness ranging between 15 and 25 m and are built up of gravel, sand, pebbly sandstone, and sandy gravel beds. The Holocene deposits comprise the unconsolidated or poorly consol dated sediments accumulated under different erosional conditions. They comprise the Nile silt and sand dunes (Table 1).

### Hydrogeology

All the previous studies had confirmed that the groundwater aquifer recorded at the fractured carbonate rocks (Faculty of Science, Beni-Suef Univ 2009). This aquifer was characterized by fractures and caves with shale contents especially

at the base and it is underlying by deep sandstone aquifer. The quality of groundwater is brackish (Table 2) and the expected productivity is ranged from low (9–20 m<sup>3</sup>/day) to medium (50–100 m<sup>3</sup>/day) depending on the depth of productive wells. In general, the depth-to-groundwater table was ranged from 40 m in the downstream of the major wadis such as Wadi El-Fagira to 110 m at small wadis over the limestone plateau. The aquifer is confined and the extracted groundwater is used for water supply such as for agriculture and other domestic means. These data were estimated and recorded from the geological and hydrogeological field data observations. This study will use these data for assisting in studying and understanding of the carbonate aquifer hydrogeophysical characteristics.

### Well data

The plotted wells in Fig. 1 were drilled by mud rotary. The max depths of these wells were ranged from 145 to 220 m and the design of these wells is not including screens except in different depths, where the shale content increased. The collected data include the locations of these wells, the total drilling depth, the depths to groundwater, the stratigraphic units which include the types of rocks units, the thickness or interface between these units and distribution of shale content, and the salinity of water and its chemical analysis. The ranges of thicknesses of the stratigraphic units at these wells are 6–25 m to the wadi deposits, 40–100 m to the marl-to-marly limestone and limestone (El-Fashn Fm.), 20–100 m to the fractured shaly limestone to limestone (Qarara Fm.) which was considered the main aquifer, and 40–80 m to the shale and limy shale which was considered extension unit to the Qarara Fm. The depths to the top of the hard limestone or to the base of the previous units were ranged from 140 to 220 m. We recorded at several wells the water level raised, in maximum, to ~25 m over the main depth to groundwater. The pumping tests reflected that the fracture density, shale

**Table 2** Values of the total resistivity ( $\rho_A$ ) of aquifer, measured T.D.S. and E.C., and calculated T.D.S., E.C., and water resistivity ( $\rho_w$ ) of groundwater and their average

Wells	$\rho$ of aquifer ( $\rho_A$ ) ( $\Omega$ m)	T.D.S <sub>m</sub> (ppm)	T.D.S <sub>c</sub> (ppm)	E.C <sub>m</sub> ( $\mu\Omega^{-1}/m$ )	E.C <sub>c</sub> ( $\mu\Omega^{-1}/m$ )	$\rho_w$ ( $\Omega$ m)
W8	40	3865.6	3651.7	6.04	5.71	1.66
W9	25	7276.8	5884.5	11.37	9.19	0.88
W10	25	5216.0	5884.5	8.15	9.19	1.23
W11	35	4128.0	4396.0	6.45	6.87	1.55
W12	40	3584.0	3651.7	5.60	5.71	1.79
W13	35	2848.0	4396.0	4.45	6.87	2.25
W14	30	4486.4	5140.2	7.01	8.03	1.43
W15	55	1868.8	1419.0	2.92	2.22	3.42
W16	30	6291.2	5140.2	9.83	8.03	1.02
Average	35	4396.1	4396.0	6.87	6.87	1.69

content, and thickness of rock units such as the shale, shaly limestone, and limy shale, which have low-to-medium effective zones (connected fractures) and affect directly on the rate of pumping or productivity of groundwater, and pure limestone, locations of wells according to the location of recorded faults and its down-throw and up-throw, and rate of pumping in governing the storages and transmissivity of the recorded aquifer Shipton et al. (2006) concluded that the fault zones in the upper crust produce permeability heterogeneities that have a large impact on subsurface fluid migration and storage patterns.

### Geoelectrical field data

In terms of electrical resistivity, one can expect that water-bearing fractured zones contrast strongly with compact bedrock. These are good targets for DC electrical imaging. In general, the apparent resistivity data of the 60 vertical electrical soundings (VESs), Schlumberger array, with max and min AB/2 ranged between 500 and 1000 m, respectively, were carried out by RIGW staff using the SAS1000 resistivity meter and collected through 3 years (2011–2014). The orientation (azimuth) of these VESs depended on the direction of wadi or perpendicular to the strike of wadi. The goals of the selected sites were for groundwater exploration and discovering different hydrogeological conditions of the expected aquifer. All these locations were chosen according to the geological and topographical features which are very important in expecting the aquifer detecting. Through this study, three transverse and five longitudinal hydro-geoelectrical profiles were constructed passing through a number of VESs and the available hydrogeological data of around seventeen productive well for showing the terrain picture of the subsurface rock unit continuity and discontinuity and their geoelectrical and hydrogeological properties (Fig. 1).

### Geoelectrical analysis

#### 1. Curve types and fault zone determination

In general, the recorded curves at this study were characterized by complicated changes in apparent resistivity values with depth and from location to other along the area. The primary comparison and guessing between these values which changes from high, low, low, high, and then low may be reflect the quaternary sediments and the marly limestone layer of the tertiary age, respectively, and their abundant curve type is QK. In addition, the same comparison was executed on the resistivity values of the tertiary age layers and revealed that the abundant curve type is KH. From the two comparisons, it concluded that the general curve type of

the penetrated subsurface geological sediments by electrical current is QKH with expecting the fractured carbonate aquifer at the end of curve type (K) and the front of curve type (H) (Fig. 2).

The determination of the fault zones is very important in hydrogeological studies, because they are interesting for appearing the continuity, discontinuity, the changes in depths, and thicknesses of the geological layers and groundwater aquifers, showing the hydraulic connection between the multi-aquifers (if recorded) either from deep or from adjacent aquifer, and increase or decrease of the fracture density with taking into account this density is more abundant and active beside these zones, especially in case of occurring of groundwater in fractured media such as fractured limestone (the studied media) or fractured basement. Bauer et al. (2016) concluded that, on a regional scale, faults of a particular deformation event have to be viewed as forming a network of flow conduits directing recharge more or less rapidly towards the water table and the springs. In addition, these faults are very important in influence positively on groundwater occurrences and acting as transmission routs in the limestone bodies' conduits for transporting and storing the included groundwater. At this study, it will focus on; how to use the resistivity method in expecting and delineating these faults and comparing with the determined faults from the geological maps using the apparent resistivity curves? The geomorphology of this area reflects and it is subjected to structure tectonics. This tectonics assisted in creating the streams (wadi), and their tributaries and the drainages system over the limestone plateau. Accordingly, it will affect on the thickness, depths, continuity, discontinuity of the subsurface geological layers, and the water-bearing layer/s and also the interconnection between this layer/s and the deep

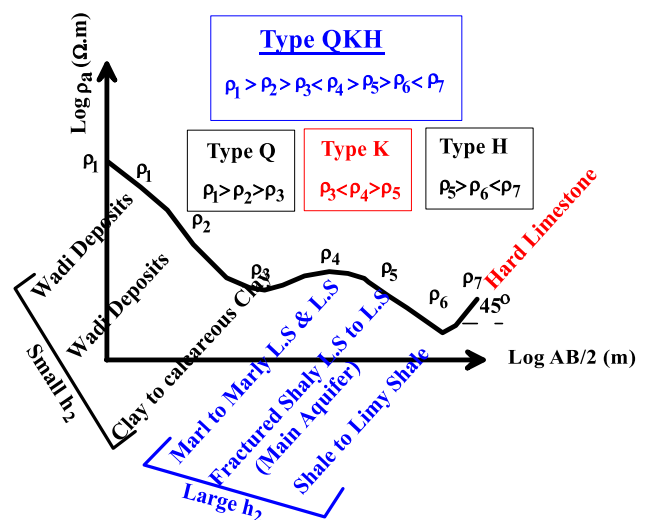


Fig. 2 Abundant curve type of the measured VESs with expecting the subsurface geological layers sequences at the study area

water-bearing layer/s. The determination of the expected locations of these faults at areas has the same conditions using this method which were difficult, because the apparent resistivities were required high accuracy in measuring and interpreting. Therefore, it must be considered that the field measurements are interesting keys in confirming the final interpretations and outputs with relying on the available geological and hydrogeological data.

Lattman and Parizek (1964) had studied the relationship between fracture traces and occurrence of groundwater in carbonate rocks and they had reported that fracture traces visible on aerial photographs are natural linear-drainage, soiltonal, and topographic alignments which are probably the surface manifestation of underlying zones of fracture concentration. They had used several bore-hole caliper surveys and these data support the concept that fracture traces reflect underlying fracture concentrations and are useful as a prospecting guide in locating zones of increased weathering, solutioning, and permeability.

The trends of these faults are interesting in controlling of groundwater occurring trapping and flowing. Atre and Carpenter (2010) reported using the seismic refraction and resistivity tomography that the faults in the limestone create permeability barriers that offset or block groundwater flowing. In addition, they are very important in selecting the potential sites for future groundwater exploration and drilling sites can be designed within the optimum distances (Solomon and Ghebreab 2008). The environmental parameters at fracturing are usually assumed to have been constant over the vertical and horizontal limits of the field, thus having little effect on relative fracture intensity variations. This leaves us with lithology and structural position as the prime factors to work with in picking optimum well locations, bore-hole trajectories, and completion zones (Nelson 2001). Parizek (1976) showed that wells on lineaments (faults) in Pennsylvanian limestone produce more water than wells that are located away from lineaments. Wells on lineaments (faults) are more likely to produce water than wells that are off lineaments (Lattman and Parizek 1964; Siddiqui and Parizek 1971). For more details about the effect of lineaments and their relation with groundwater occurrences in karstic area, see Kazemir et al. 2009 and Frohlich et al. 1996. They had reported that a geoelectrical depth sounding, on the other hand, was interpreted by assuming a horizontally layered model. Any nearby lineament would be expected to cause lateral resistivity effects. Lateral in-homogeneities usually cause the apparent resistivity values to be scattered, making the resistivity curves unsteady or noisy. Sometimes, the curves are steady, but the best-fitting layer models demand unreasonable layer resistivities. Therefore, the determination of faults and how to expect and determine these faults are very complicated and very interesting in studying the hydrogeological properties of aquifer. In some cases, fault zones

are also associated with bedrock depressions and thicker accumulations of unconsolidated sediment (Atre and Carpenter 2010).

At this study with calibrating the recorded fault locations from geological investigations, the apparent resistivity curves of VESs will be used in determining the expected zones and locations of faults as first assumption before carrying out the inversion of these curves for confirming that. Where the two apparent resistivity curves to each two adjacent VESs will be mapped to show and predict the existence or non-existence faults according to the new following assumptions:

- (a) When there is coinciding or diverging between the measured curves of two adjacent VESs, it will be expected that the recorded subsurface layers had been continuing horizontally and their expected recording depths according to AB/2 had been symmetrically and there is no fault between both (Fig. 3).
- (b) When there is intersecting between the curves of each two adjacent VESs, it will be expected that there is fault between both and the intersect point of the two curves is the peak of this fault or the beginning depth to detect the fault. This will give indication about the determination of the intersect point and its expected depth according to AB/2 is very important for forward modeling and in determining the depth to the peak either shallow or deep for this fault from the surface. In addition, after intersecting and reversing of each two curves, it can predict the down-throw and up-throw of this fault (Fig. 4a–l).

These assumptions were applied at this study and concluded that there are several subsurface inferred faults (dashed lines) (Fig. 8), and they are considered as major fracture traces. Those faults were confirmed by the field observations and geological maps and also from inversion of the resistivity field data (Fig. 7). Those faults show as extension to the observed and mapped geological faults (solid lines), especially to the east of the area. Therefore, those faults assisted in understanding the complicated hydrogeological conditions of this area. Ganerød et al. (2006) reported that in most cases, 2D resistivity clearly identifies zones in the bedrock that can be observed as fault and/or fracture zones and the results showed a good correlation between the resistivity profiles and mapped structures on the surface. On map (9), there are two traces of faults, the first is solid and the second is dashed. The solid faults had delineated from the geological map, while the dashed faults were inferred and delineated from the geoelectric data.

Therefore, the occurring of those faults will affect the topographic features (elevations and slope of these features (Figs. 10, 11), groundwater occurrences, depths and flowing

**Fig. 3** Coinciding and/or diverging between the different VESs using the field apparent resistivity measurements

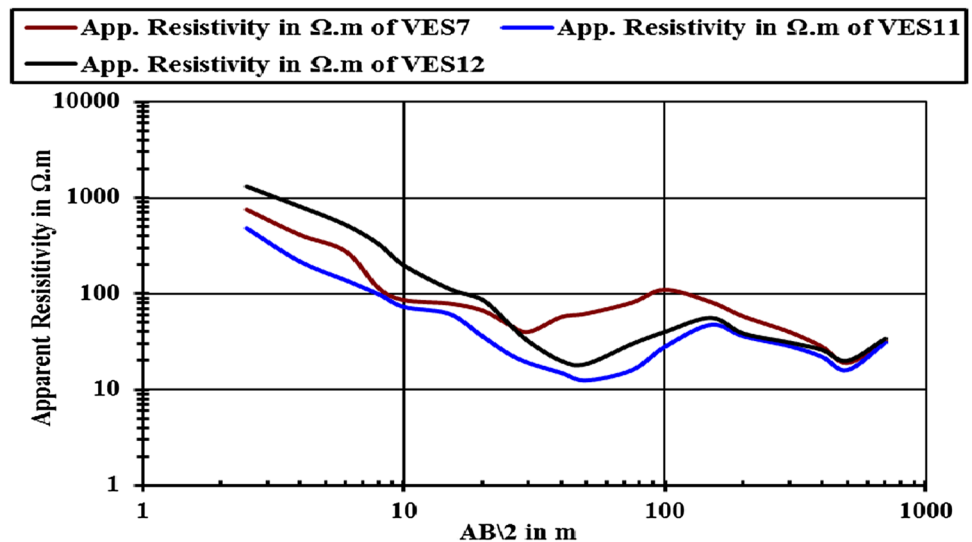


(Fig. 12), and the expected recharging of the recorded aquifer either from deep aquifer or from surface (rainfall). This phenomenon was detected at the wells to the northeast direction, where the several recorded and dissected faults especially at the location of the up-throw of faults. We were monitored that the productivity of the wells at this location was 5–7 m<sup>3</sup>/day, but the productivity of the wells to the east and west was  $\geq 60$  m<sup>3</sup>/day. In addition, those faults will be very important in expecting, decreasing, and increasing of the fractures density or assisting in generating of these fractures which are considered the main pores or channels for including and transporting the groundwater through the fractured aquifers. Therefore, map 12 illustrates that the shallow depths of groundwater were occurred, in general, at the locations where the down-throw of faults. In addition, It is believed that those faults affected in groundwater flowing.

## 2. Hydro-geophysical characteristics

In general, the quantitative interpretation of the field data was carried out interpretation of the vertical electrical sounding curves depended on Zohdy's technique (1989), for preliminary interpretation, and the Rinvert software (1999) for final inversion for estimating the terrain resistivities, which are assisting in predicting the hydrogeological properties of the recorded layers with depths. From this interpretation, it can detect that the lithologies encountered within these layers in the vicinity of the analyzed VESs and between them and confirming of the expected inform of inferred faults. This may reflect the vertical and lateral changes in the rock constitution of the shallow section penetrated by the electric current. The determination of the terrain resistivities of the different subsurface layers can give good information about the saturated fractured layers and their fractures density and groundwater, as well as their properties and their affects of

electrical current impedance and/or conductance. Frohlich et al. (1988) were reported from resistivity studies that metamorphic pelites and limestones yielded low resistivities over high-yield fractured rock. Frohlich et al. (1996) were reported that the bedrock generally shows low resistivities if it is fractured and if the fractures are interconnected. It is based on assumption that various entities such as minerals, solid bedrock, sediments, air, and water-filled structures have detectable electrical-resistivity contrast relative to the host medium (Pánek et al. 2010). At this study, it was supposed that considerable resistivity contrasts between hard limestone bedrock, the saturated limestone, saturated shaly limestone, and shale zones can be detected. Robert, et al. (2011) concluded that using ERT and SP methods for using in locating water-bearing fractures in limestones depending on detect and characterize (in terms of direction, width, and depth) fractured zones expected to be less resistive, the wells drilled in conductive or low resistive zones and/or in SP anomalies have high yield, but the wells drilled in resistive zones and/or outside SP anomalies have poor yield. In addition, Zhu, et al. (2011) used three types of resistivity techniques (surface 2D survey, quasi-3D survey, and time-lapse survey) to map and characterize resistivity anomalies in karst aquifer. They found that the drilling results also suggest that low-resistivity anomalies in general are associated with water-bearing features. Khaled et al. (2016) and Redhaounia et al. (2016) showed the low resistivity of cavities in the limestone rocks and the highly fractured and karstified limestone which are saturated by the groundwater. However, differences in the anomaly signals between the water-filled conduit and other water-bearing features such as water-filled fracture zones were undistinguishable and the electrical-resistivity method is useful in conduit detection by providing potential drilling targets. Ganerød et al. (2006) compared among 2D resistivity, refraction seismic, and VLF for



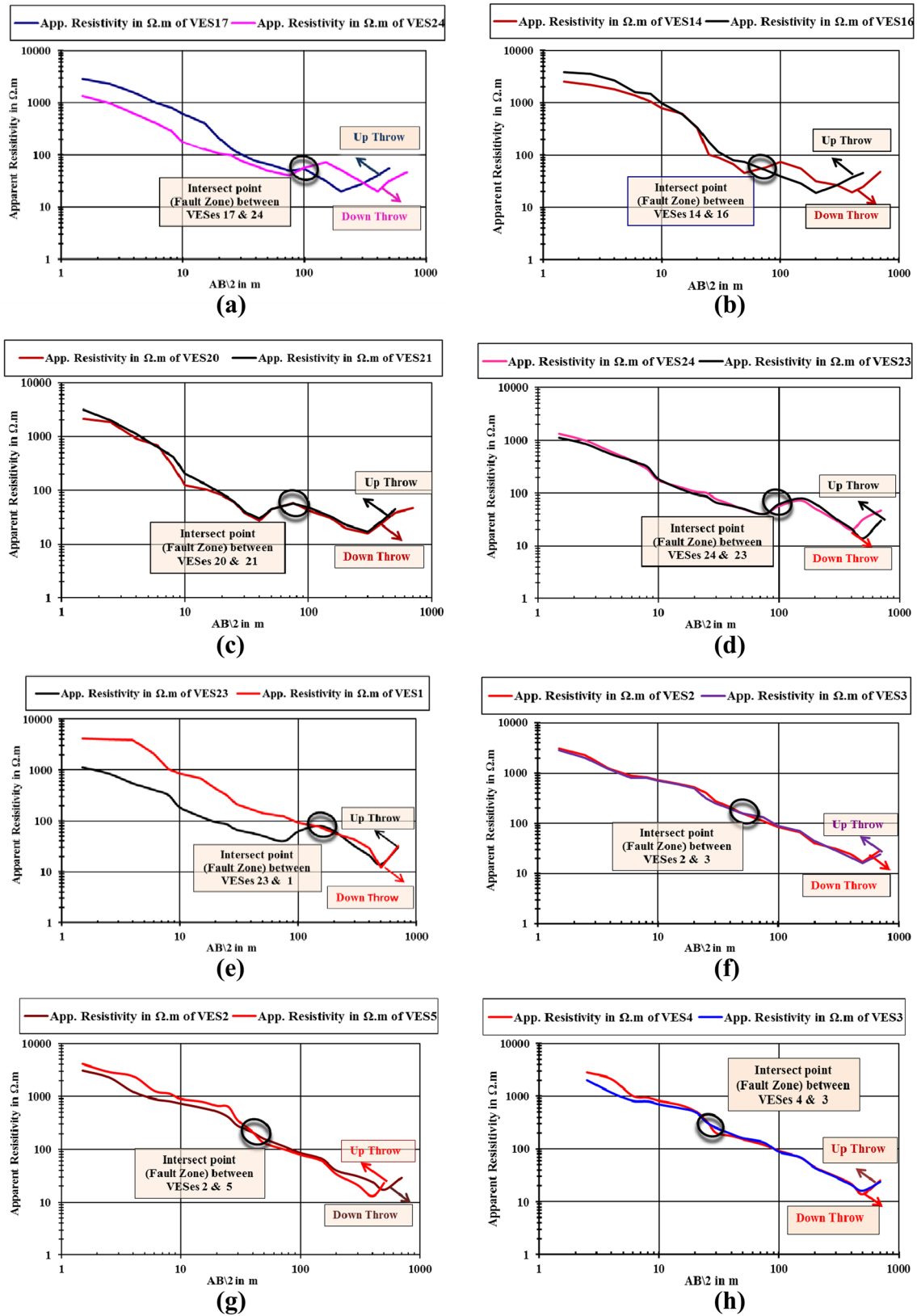


**Fig. 4** Expected fault zone determination at expected shallow depths (a–i) and expected deep depths (j–l) according to AB/2 between the different VESs using the apparent resistivity measurements

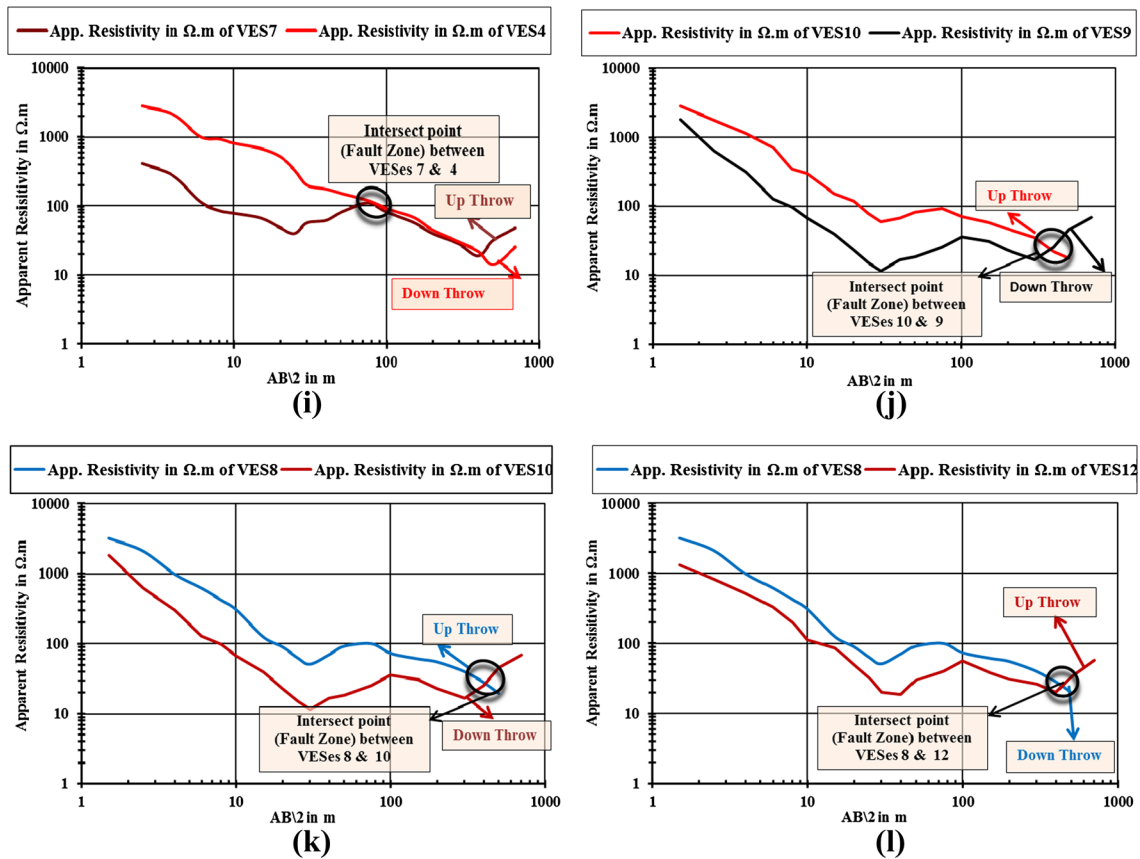


Fig. 4 (continued)

subsurface mapping of faults and fracture zones and showed that 2D resistivity data are most valuable for interpreting geological structures in the subsurface. With 2D resistivity, the position of a zone is well-identified. This method may also provide information on the depth and width of the zone as well as the dip direction.

The results of VESs assisted in building of eight hydro-geoelectrical profiles along the study area (Fig. 1) and the general hydro-geoelectrical imagination to the recorded subsurface layers was reported on the profile A–A (Fig. 5), where revealed that the number of layers was seven. These results were confirmed by the geological and hydrogeological data of 17 wells, the exposed rocks (Fig. 6) (with concentrating on the saturated layers and this confirming the area was subjected to high structure tectonics), and also according to the measured multi-types curve (Fig. 2). Accordingly, the reported lithologies of the recorded geoelectric layers were formed from wadi deposits (first and second geoelectric layers) and clay to calcareous clay (Quaternary age) and sometimes transformed to marl of the third layer, while the layers from fourth to seventh were made up of marl-to-marly limestone and limestone, shaly limestone to limestone, shale to limy shale, and hard limestone rocks [tertiary age (Middle

Eocene)]. In general, the resistivity values of clay are ranged between 2 and 40 ( $\Omega$  m), limy shale and shale values are ranged from 2 to 22 ( $\Omega$  m), while the fractured limestone and fractured shaly limestone are ranged between 11 and 93 ( $\Omega$  m). In addition, the resistivity values of wadi deposits are varied from 69 to 5323 ( $\Omega$  m), marl and marly limestone are varied from 38 to 162 ( $\Omega$  m), while the values of hard limestone are ranged between 76 and 848 ( $\Omega$  m). Therefore, the estimated terrain resistivities of these layers reflected the following hydrogeoelectric properties:

- The wadi deposits and clay to calcareous clay are dry because of their high impedance to the electrical current.
- The marl-to-marly limestone and limestone rocks (*El-Fashin formation*) are also dry.
- The fractured shaly limestone-to-limestone rocks (*Qarara Formation*) are saturated with groundwater and considered the main aquifer because of their low impedance to the electrical current. The lowering in resistivity value (11  $\Omega$  m) of this aquifer may be resulted from increasing of the shale content and salinity of water pores, while the intermediating value

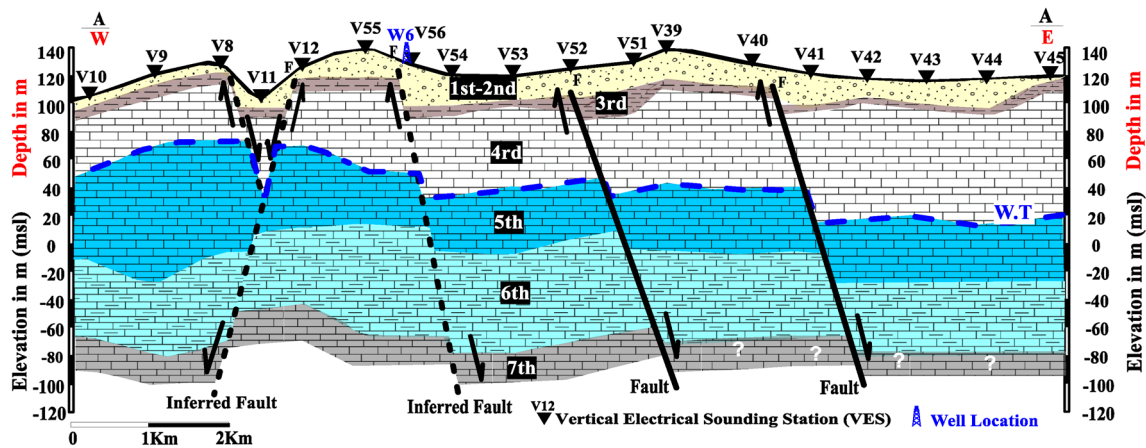
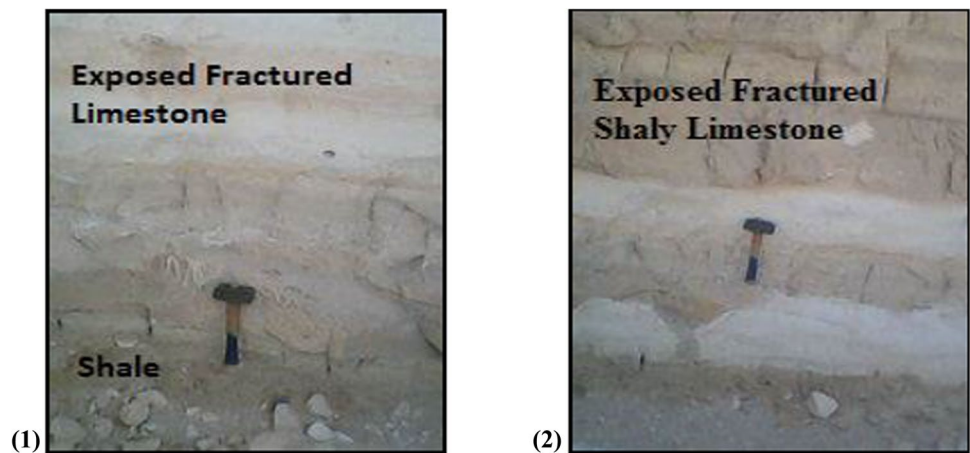


**Fig. 5** Hydro-geo-electrical profile (A–A). *First and second layers* dry-to-wetted wadi deposits (quaternary age) (67–2699 Ω m). *Third layer* clay to calc. Clay and Marle (quaternary age) (2–38 Ω m). *Fourth layer* Marle-to-Marly L.S and L.S (El-Fashn Fm.) (Tertiary Age, Middle Eocene) (18–132 Ω m). *Fifth layer* fractured shaly L.S to

limestone (main aquifer) (Qarara Fm.) (Tertiary Age, Middle Eocene) (20–62 Ω m). *Sixth layer* shale to limy shale (Qarara Fm.) (Tertiary Age, Middle Eocene) (2–20 Ω m). *Seventh layer* hard limestone (Tertiary Age, Middle Eocene) (100–144 Ω m)

**Fig. 6** Photos at the study area show the fractures at the exposed main rocks of the fractured aquifer



(93 Ω m) is depending on the occurrence of water into the fractures. In addition, the low value indicated about increasing in fractures density and medium content of shale with high soluble salts in the water content. The medium value reflects the increase in fracture density with fresh water and minor content of shale.

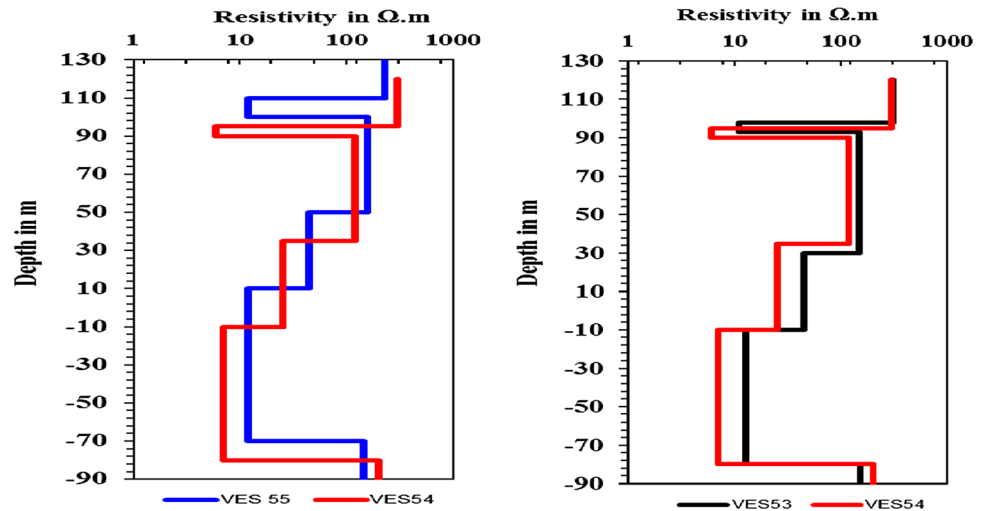
- (d) The limy shale rocks to shale are considering as extended layer to the main aquifer (Qarara Formation) at different locations. Their impedance for the electrical current penetration was very low, because the shale was wetted and its water content was saline, to low because the shale content is decreased, and the water content in fractures is brackish water.
- (e) The limestone rocks were hard and dry, because there are no fractures.

Along this profile, there are inferred and detected faults between different VESs. The existence of the inferred faults was confirmed after inverting of the apparent resistivity curves and also confirmed that the previous assumption which concentrated on intersecting between the two adjacent VES curves reflects the existence of faults. Figure 7 shows the existence and non-existence faults between the two adjacent VESs.

(A) Terrain-resistivity ranges

Hardening of rock by compaction and/or metamorphism will reduce porosity and permeability and hence increase resistivity. Resistivity is, therefore, an extremely variable parameter, not only from formation to formation, but even within a particular formation. There is no general correlation of lithology with resistivity. Nevertheless, a broad

**Fig. 7** Intersecting and shifting between the inversion curves of VES 54 and VES 55, *to left* for showing and confirming the fault between both, while there are no intersecting and shifting between VES 54 and VES 53, *to right* for showing, there is no fault between both



classification is possible according to which clays, shales, sands and gravel, compact sandstones and limestones, and unaltered crystalline rocks stand to increase resistivity (Sharma 1997).

The estimated terrain-resistivity ranges of the carbonate aquifer at this area are very important for classification of the expected density of fractures and in expecting the hydrogeological properties of the aquifer such as the porosity, hydraulic conductivity, groundwater potentiality and their quality, and so on. Those ranges will be important during study of the carbonate aquifer at North Africa and especially at the east desert and west desert of Egypt with taking into account the geological conditions. The determination of the previous aquifer properties requires separating the lithologic constituents and its distribution such as the shaly and non-shaly contents because of the high effect of shalenss on these properties and, therefore, water quantity and quality. Therefore, the shale-to-shaly limestone, highly fractured shaly limestone, highly fractured limestone and fractured limestone terrain resistivities ranges were determined. These ranges are 2–22 ( $\Omega$  m) for the shale to shaly limestone, 11–20 ( $\Omega$  m) for the saturated highly fractured shaly limestone-to-limestone, 20–50 ( $\Omega$  m) for the saturated highly fractured limestone, and 50–93 ( $\Omega$  m) for the saturated fractured limestone (Fig. 8) as correlated with the hydrogeological data.

In general, the terrain-resistivity values of the fractured limestone, limy shale, and shale rocks were mapped for understanding the distribution of the pure carbonate rocks and shale content at these layers for assisting and predicting the distribution of the effective fracture zones and the fracture density and expecting the locations of high groundwater accumulation. Therefore, the distribution of the resistivity values of the fractured limestone rocks (Fig. 9) appeared differentiations in values from low in several locations to intermediate at the others. Where the low-resistivity values,

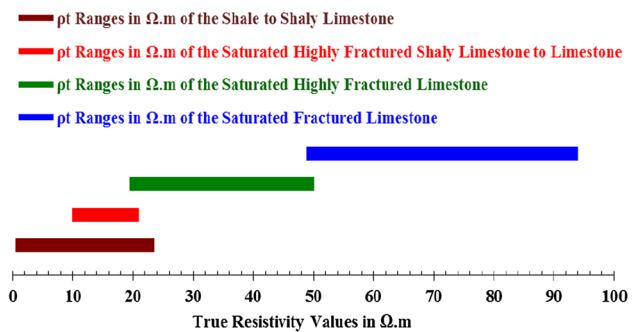
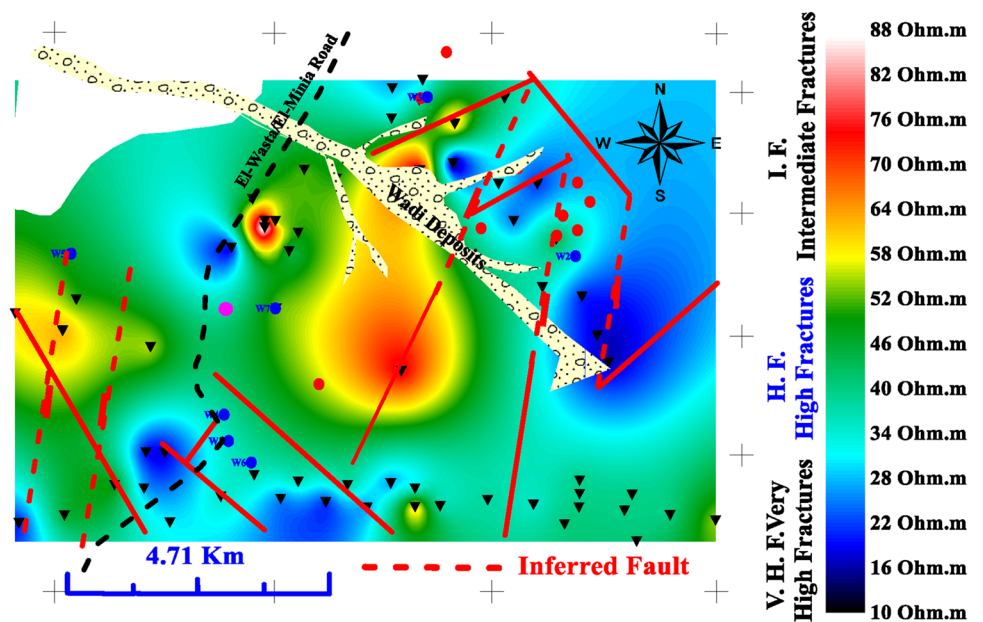


**Fig. 8** Ranges and overlaps between the terrain-resistivity values of the water-bearing layers and shale layer

which are ranged from 11 to 50 ( $\Omega$  m), reflect the locations of very high fractures (V.H.F) and high fractures (H.F) and refer to the probability in increasing of fracture intensity and density. Accordingly, the water accumulation will be high and its water quality is expecting brackish to fresh and may refer to occurrence of fractures, fissures, joints, vugs, and caves. While the medium values, which are ranged between 50 ( $\Omega$  m) and 93 ( $\Omega$  m), may refer to the relative decreasing in fractures density and intensity and water content of the carbonate rocks and its water quality is fresh. Therefore, these rocks will classify under the intermediate fractured (I.F) rocks (Fig. 9).

On the terrain-resistivity distribution map of the fractured limestone (Fig. 9), the values of this resistivity are decreasing at the expected locations of very high fractures and high fractures. This referred to depend the electrical current penetrating of the considered section of carbonate aquifer on the density of pore system and its water saturation percentages. It can be concluded that the fracture intensity or density, and their water saturation will increase at these locations. Consequently, the groundwater accumulation is expected high and its quantity is expected more suitable for yielding with

**Fig. 9** Terrain-resistivity distribution map of the fractured carbonate aquifer

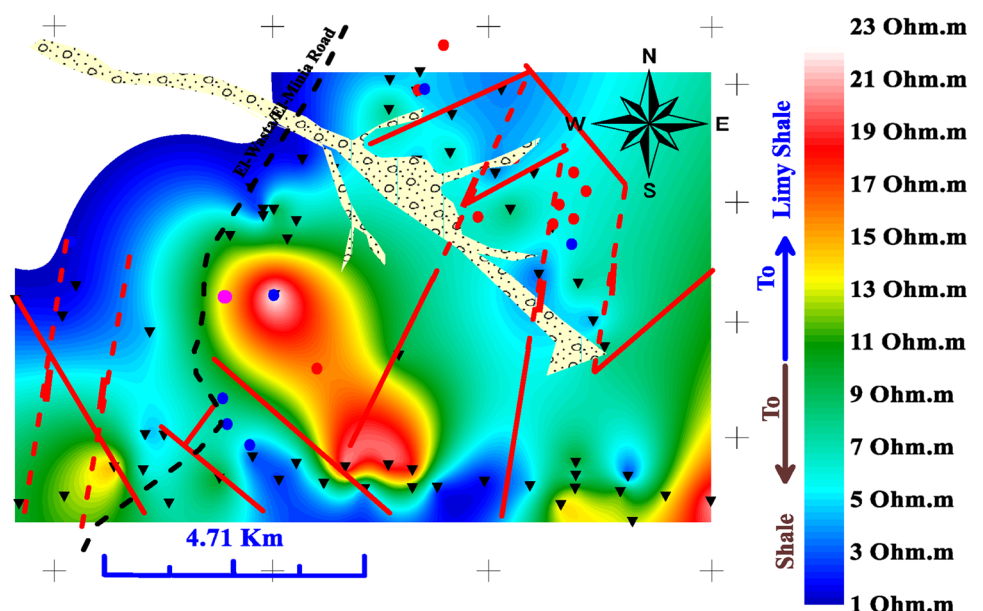


expectation increasing in minor content of shale and salinity at these locations. While the other locations of intermediate resistivity values, especially from the center to the west of the area, may refer to low fracture intensity or density and also low in groundwater accumulation with expecting in increasing of calcium carbonate ( $\text{CaCO}_3$ ) and caves or vugs. The last locations may and expect have less quantity and productivity in groundwater and characterized by brackish to fresh water depending on decreasing and increasing of their resistivities, respectively.

The terrain-resistivity distribution of the limy shale and shale rocks at this area (Fig. 10) displayed three locations

of limy shales, but the other locations included the pure shale. The limy shale is more condensing at the central locations taking axis directed northwest–southeast adding to small locations at several parts. These values reflect that the sediments are fractured and may be including intermediate-to-high shale content. Therefore, these locations are including low-to-medium reducible water content and their quality is brackish to saline and their productivity is low to medium because of the presence of high content of shales. At this case, these locations shall be considered as extending aquifer to the main aquifer. The construction of

**Fig. 10** Terrain-resistivity distribution map of the limy shale and shale rocks



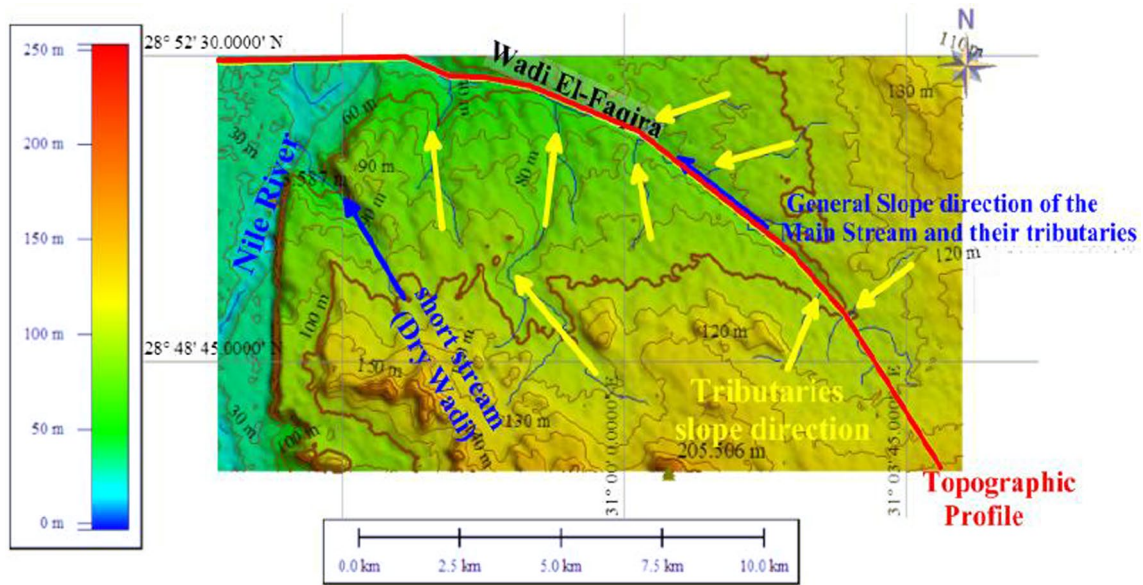
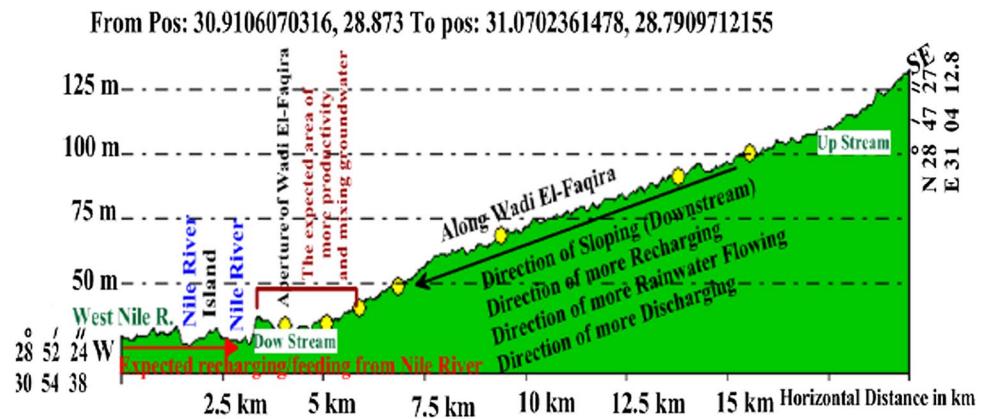


Fig. 11 Topographic map of the study area using Global Mapper v11

Fig. 12 Topographic profile passes through the main wadi (Wadi El-Faqira) using Global Mapper v11



this map was very important in showing the distribution of shale layer as base to the main aquifer.

(B) Expected groundwater flow

In general, before showing the depths to groundwater and main aquifer, it must be studying the different topographic features of the study area such hills, mountains, and streams (dry wadis), because these features are interested in expecting the shallow and deep depths of aquifer, the continuity and discontinuity of geological layers, and the locations of recharging.

In arid regions, groundwater is recharged only from the scanty local rainfall plus water that enters as streams or via artesian aquifer. Khaled et al. (2016) concluded that fractured aquifer is recharged via the percolation of the surface runoff water through the fracture lines, fault planes,

and bedding planes besides paleowater of the paleo-rainy seasons. Deep groundwater may be very old and a relic of former times when evaporation rates were reduced by lower air temperature useful supplies, nevertheless, is often small and the water table generally lies well below the surface. Under these conditions, if recharge is not kept in balance with the rate of withdrawal, further drawdown of the water table will occur, and these valuable natural resources may be depleted. In general, the main order of stream at this area is the fourth order. The arrangement and dimensions of streams in a drainage basin tend to be orderly. This can be verified by examining a stream system on a mapping and numbering the observed stream segments according to their position, or order, in the system. The smallest segments, without tributaries, are classified as first-order stream. Those with only first-order tributaries are second-order streams, while third-order streams have first- and second-order tributaries. If the

frequency of segments of each order is then tabulated, it can quickly be seen that for any stream system, the frequency of segments increases with decreasing stream order. In other words, a stream system is somewhat like a tree, with a trunk and numerous branches. There is only one stream segment of the highest order (the main stream as mapped in Fig. 11), but there are many tributaries, with their numbers increasing, the shorter they are. These order lines are like inherent in a stream long profile, in which gradient decreases systematically from head to mouth, while discharge, velocity, and channel dimensions increase. All these relationships imply that in response to a given quantity of runoff, stream systems develop with just the size and spacing required to move the water off each part of the land with greatest efficiency (Skinner and Porter 1987). Bore-hole logs suggested that the low-velocity values are caused by low rigidity fractured and vuggy rock, water zones, cavities, and collapse features. Surface streams tend to lie directly above the low-velocity zones, suggesting fault and fracture control of surface drainage, in addition to the subsurface flow system (Atre and Carpenter 2010).

Therefore, the study area is considered a part of the Middle Eocene plateau which characterizes with contour levels ranged from +70 to +255 m (+msl) and dissected by some wadis such as wadi El-Faqira and their tributaries (Fig. 11). These plateau and wadis were covered by alluvial and alluvium deposits (wadi deposits). The thickness of these deposits is ranging between 15 and 25 m. The source or head of this wadi is from southeast and its mouth is to northwest where Nile valley. This reflected its general sloping which is from southeast to northwest as delineated on the topographic map (Fig. 11) and topographic profile (Fig. 12). The dendritic pattern is the main drainage type which characterized wadi El-Faqira, as shown in Fig 11.

Topographic profile (Fig. 12) appears that the main sloping of Wadi El-Faqira, rainwater flowing direction or flooding, expected direction of recharging of aquifer, and the expected direction to the areas of more productivity is from southeast (Plateau) to northwest (Nile valley). In addition, this profile appears that the main aquifer may be recharged by rainwater from this wadi and from Nile River especially at downstream. These features may effect and reflect directly on the depths to groundwater and on the expected areas of more groundwater occurrences, accumulation, and fracturing. Meir et al. (2007) concluded that, using the integration between geophysical and hydraulic data, it can delineate of the main flowing features and showed that such features are directly or indirectly linked to karst phenomena. Ford and Williams (2007) found that poorly understood to the spatial and temporal complexities of the flow patterns into the carbonate aquifer caused by widely varying porosity and permeability and the organization of the conduit and matrix system. Understanding this complex flow system is critical

for an appropriate assessment of groundwater resources and the design of sustainable groundwater production schemes. Most of the previous conditions occur on map 13, where the shallow depths to groundwater were recorded along wadis and the groundwater flow is expected from southeast to northwest according to the general sloping of wadis.

Accordingly, the distribution of depth-to-groundwater aquifer (Fig. 13) and its relation with topographic conditions of the study area concluded that the direction of recording shallow depth to groundwater is more conjunction with the general sloping of the surface and the main streams which is expected from southeast to northeast. In addition, it can be expected that the groundwater aquifer recharging, flowing, and accumulating have the same direction of general sloping. According to Ammar and Monem (2011) assumption, the decreasing direction in resistivity values of the effective zones (clean zones) of the aquifer can give good indication about the expected groundwater accumulation and flowing. This assumption was applied at this study and confirmed that there is matching between the delineated flow direction from the hydrogeological data, (depth to groundwater, red arrows, and porosity values, magenta arrows) and from the geoelectrical data (green arrows), as shown in Fig. 13. This flowing seems more complicated because of subjecting of the area to structure tectonics. This complication in groundwater flowing (Fig. 13) reflects and confirms the effect of fault and fracture zones on the dynamics of water through fractures of the aquifer and as indicator to the groundwater resources.

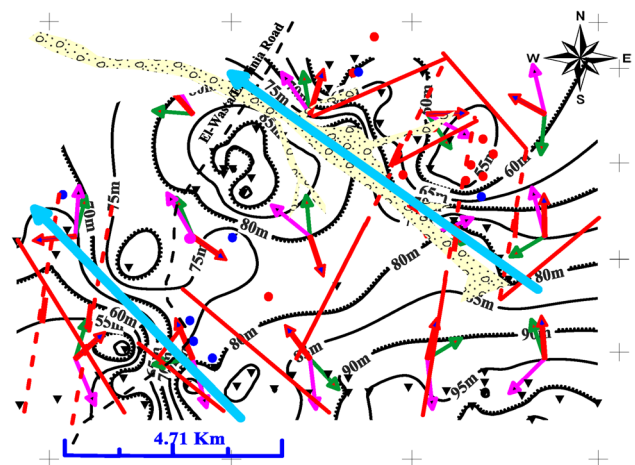


**Fig. 13** Expected directions of groundwater recharging and flowing distribution map according to resistivity outputs of the pure fractured carbonate aquifer and wells data. The black lines are the direction of recording shallow depths of groundwater, general sloping, and sloping of the main wadis. The red arrows (from groundwater depths distribution) and green arrows (from resistivity outputs) are the expected directions to the areas of shallow depths, groundwater recharging or accumulation and flowing. The magenta arrows reflect the increasing of porosity

(C) Relationship between the electrical resistivity/conductivity ( $\rho_w/EC$ ) of water, total dissolved solids (T.D.S.), and the resistivity of aquifer ( $\rho_A$ )

Serra (1984) had reported that the resistivity of rocks and sediments is controlled by a number of factors, the most important of which are:

1. The resistivities of the water ( $\rho_w$ ) in the pores (fractures) vary with the nature and concentration of its dissolved salts (T.D.S.).
2. Quantity of water present; that is, the porosity (at this area is secondary porosity) and the saturation.
3. The lithology (at this area is limestone to shaly limestone), i.e., the nature and percentage of clays present and traces of conductive minerals.
4. The texture of the rock; i.e., distribution of pores (at this area is random and varied in types), clays (at this area is shaly limestone, limy shale to pure shale at the base), and conductive minerals.

Therefore, for showing the effecting of these factors on the resistivity of the carbonate aquifer, the statistical analysis between this resistivity and T.D.S. was carried out by the MINITAB (1998) statistical software package for deducing the relationship between two variables and appearing the effect of salinity on the bulk resistivity. This package was used for fitting the data to obtain an optimal estimation of the model's parameters. The outputs of this program included the descriptive statistics (Figs. 14, 15), parameter estimation, statistical hypothesis testing, and the basic linear regression which consists of linear regression, analysis of variance (ANOVA) table, and model fit validation (Figs. 16, 17). The relationship between any two variables will be deduced by

applying the previous statistical concepts especially for the carbonate aquifer at this study which is controlled by several factors such as porosity (fractures) including the density of fractures, TDS, water resistivity, shale content, and amount of water.

In general, decreasing the aquifer resistivity ( $\rho_A$ ) gave indication about increasing of T.D.S. ( $\rho_A \propto 1/T.D.S.$ ). By judging the previous relationship, the distribution was normal and identical, the general trend of the data was linear, and the model fit was valid. However, because the *T*-ratio and *F*-statistic values were high, the *P*-probability value was decreased to 0.005. This reflects that the evidence between the two variables is strong and this relationship is different and the correlation between these variables is high ( $-0.833$ ; *P* value = 0.005) (Fig. 16). There is a strong evidence of a relationship between both and this relation is linear and it means that the measured T.D.S.m differ significantly for different  $\rho_A$  ( $\Omega$  m). *R*<sup>2</sup> of the two variables is around 69.3% that refers to  $\rho_A$  ( $\Omega$  m) of the carbonate aquifer at this area cannot be interpreted more than 69.3% of T.D.S. or around 30.7% of T.D.S. cannot be interpreted by  $\rho_A$  ( $\Omega$  m). This resulted from the effect of shale distribution, connection, and saturation percentages of the pores, the distribution and density of these pores, and their different types such as vugs, caves, fractures, joints, and fissures add to the other previous factors. Hence, it can use the following linear regression for estimating T.D.S. from  $\rho_A$ :

$$T.D.S. = 9605.69 - 148.846(\rho_A). \tag{1}$$

During the application of the previous empirical formula (1), it must take into account that the T.D.S. is ranged between 1800 and 8000 (brackish water) and the resistivity values of aquifer are ranged between 25 and 55  $\Omega$  m. These conditions must be followed during applying the resulted

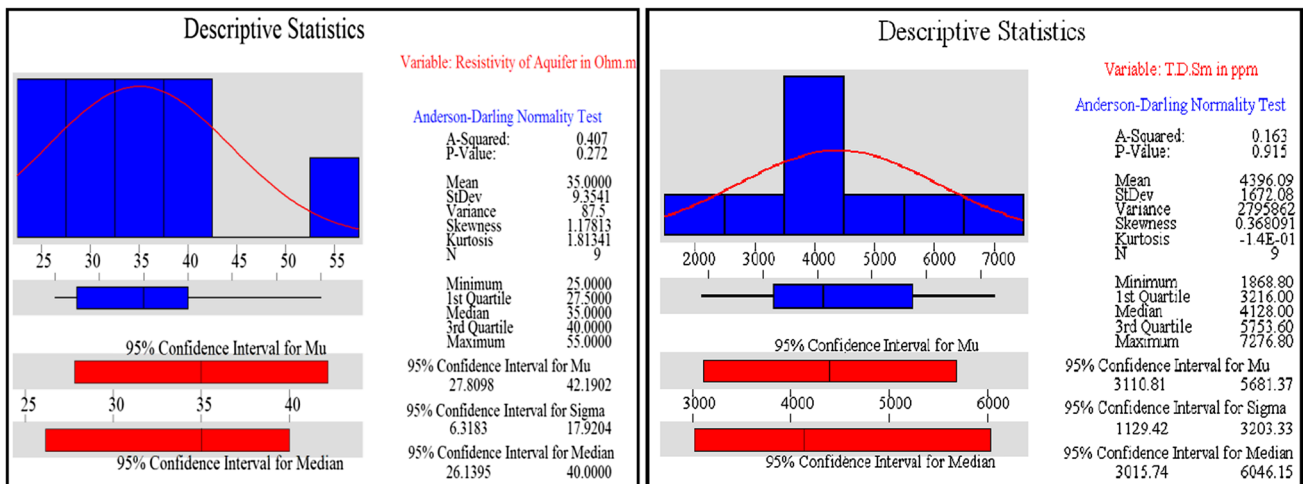


Fig. 14 Descriptive statistics of the terrain resistivity of carbonate aquifer (left) and T.D.S. of water (right)



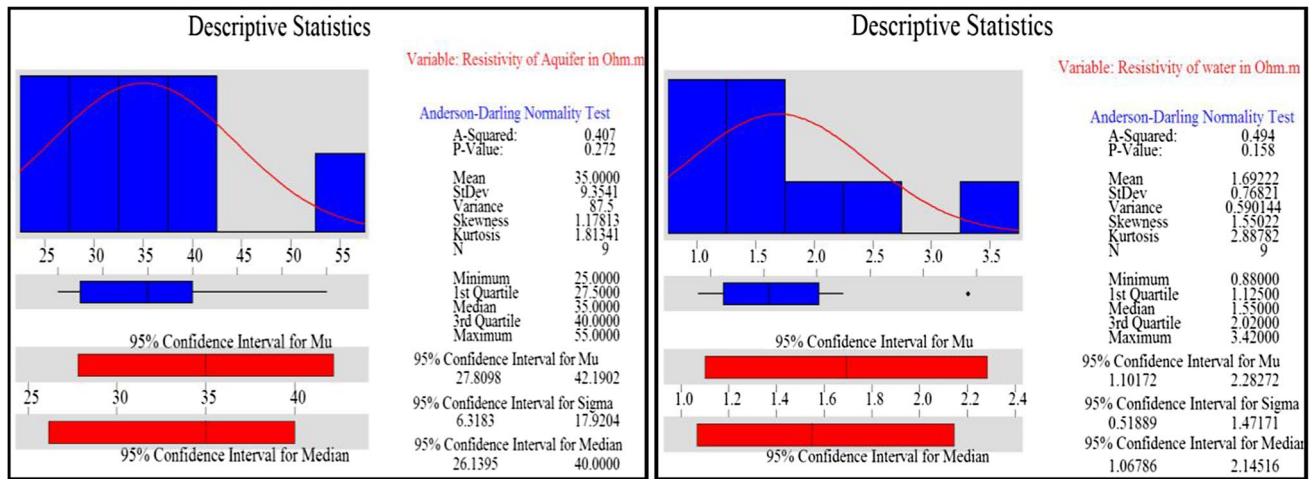


Fig. 15 Descriptive statistics of the terrain resistivity of carbonate aquifer (left) and resistivity of water (right)

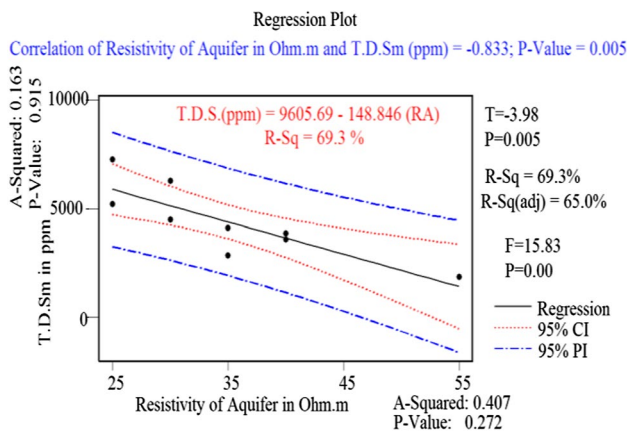


Fig. 16 Relationship between of the terrain resistivity of carbonate aquifer and T.D.S. of water

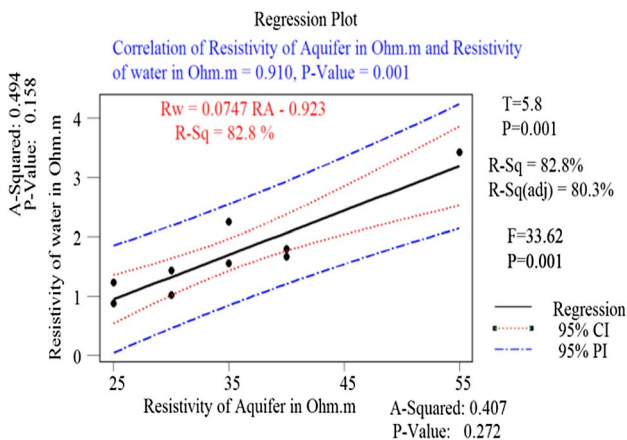


Fig. 17 Relationship between the terrain resistivity of carbonate aquifer and resistivity of water

empirical formula (2) between the aquifer resistivity ( $\rho_A$ ) and the water resistivity ( $\rho_w$ ).

In addition, from the relation between resistivity of aquifer and resistivity of water (Fig. 17), the resistivity of aquifer increases with increasing the resistivity of water ( $\rho_A \propto \rho_w$ ) and vice versa. The distribution of this relationship is normal and identical, the general trend of the data is linear, and the model fit is valid. However, because the  $T$  and  $F$  values are high,  $P$  value decreases to 0.001. This reflects that the evidence between the two variables is strong and this relationship is different.

The correlation between the two variables is high (0.91;  $P$  value = 0.001) (Fig. 17). There is a strong evidence of a relationship between both and this relationship is linear and it means that  $\rho_w$  differ significantly for different  $\rho_A$ .  $R^2$  of the two variables is around 82.8 that refer to  $\rho_A$  of the carbonate aquifer cannot be interpreted more than 82.8% of  $\rho_w$  or around 17.2% of  $\rho_w$  cannot be interpreted by  $\rho_A$  of the aquifer. This may be from the effect of shale content, connection, and saturation percentages of the fractures and their densities and distribution. Hence, it can use the following linear regression for estimating  $\rho_w$  from  $\rho_A$ :

$$\rho_w = 0.0747\rho_A - 0.923. \tag{2}$$

According to the previous factors, the resistivity of the recorded carbonate aquifer is more affected by the electrical resistivity or conductivity of water into the fractures. This affecting is more varied with varying the nature and concentration of the T.D.S., which are high (Table 2). According to the previous statistical analyses between the previous estimated three parameters at this study (Figs. 14, 15, 16, 17), the resistivity of aquifer decreases with increasing the total dissolved solids ( $\rho_A \propto 1/T.D.S.$ ), but it increases with increasing the resistivity of water ( $\rho_A \propto \rho_w$ ). At the end, we

can said that the resistivity of water and T.D.S. of the water are considered the main effect and more affecting on the bulk resistivity of the aquifer, but they may reduce the effect of other parameters such as porosity, permeability, and shale content on the bulk resistivity of aquifer which may range from 17 to 31%.

#### (D) Porosity calculation

The secondary porosity, which is made up of vugs caused by dissolution of the matrix and fissures or cracks created by mechanical forces (weathering or structure tectonics such as faulting), is a common feature of rocks of chemical or organic origin and developed after the phenomena of deposition, compaction, and cementation. The effective porosity ( $\phi_{\text{eff}}$ ), which is accessible, to free fluids and excludes non-connected porosity and the volume occupied by the clay-bound water or clay-hydration water surrounding the clay particles. The last porosity type may be much lower than the total porosity when the pores in a rock are not interconnected (pumice stone) or when the size of the pores is such that the fluids cannot circulate or even when a part of the water is absorbed by the minerals in the rock (clay) (Serra 1984; Chapellier 1992).

In general, porosities tend to be lower in deeper and older rocks. This decrease in porosity is primarily due to the cementation and overburden pressure stresses on the rock. There are many exceptions to this general trend when normal overburden conditions do not prevail. The secondary porosity includes vugy porosity that acquired as a result of dissolution, fracture porosity, and intergranular produced due to weathering. These secondary porosities are developed after the processes of deposition, compaction, and sedimentation (Chapellier 1992). Several geological parameters are important in controlling fracture spacing in subsurface rock units that are composition, grain size, porosity, bed thickness and structural position, and the relative fracture spacing can be predicted through the analysis of these parameters. In general, relatively stronger, more brittle rocks will contain closer-spaced fractures. Therefore, any parameter that strengthens or embrittles a rock will increase its fracture intensity during deformation. The porosity and permeability of natural subsurface fracture systems are a function of fracture spacing or intensity (how many fractures? fracture/m) and fracture aperture available for fluid flow (how wide they are?). The environmental parameters at fracturing are usually assumed to have been constant over the vertical and horizontal limits of the field, thus having little effect on relative fracture intensity variations. This leaves us with lithology and structural position as the prime factors to work with in picking optimum well locations, bore-hole trajectories, and completion zones (Nelson 2001).

Frohlich et al. (1996) were reported that not every lineament was found to be associated with high fracture density and high hydraulic conductivity. In addition, they were correlated the high values of hydraulic conductivity with low bedrock resistivities, and in some cases, very low resistivities were confined to the upper part of the bedrock (weathered), where the hydraulic conductivity was very large. The lineaments were used to guide a drilling program with the intention of penetrating as many fracture zones. Although the VES curves can be interpreted in terms of horizontal layers, the presence of vertical fracture zones may lower the horizontal layer resistivities or suggest a thickness of the low-resistivity bedrock aquifer that is too high. Therefore, at this study, we concentrated on delineating and how to use the resistivity data in detecting the faults which may lead to the expected area of high fractures, groundwater accumulation, and the feeding of aquifer. Parizek (1976) showed that wells on lineaments (faults) in Pennsylvanian limestones produce more water than wells that are located away from lineaments. Wells on lineaments (faults) are more likely to produce water than wells that are off lineaments (Lattman and Parizek 1964; Siddiqui and Parizek 1971). Therefore, the hydraulic conductivity/fracture intensity will expect to increase with decreasing the resistivity in the areas near the faults. Ammar (2013) reported that the resistivity decreases with increasing the density of fractures at the fractured basement aquifer which leads to direct effect of fracture on the aquifer resistivity. In addition, the resistivity can use in expecting the fracture density, porosity then hydraulic conductivity.

In general, the carbonate aquifer often has solution features that resulted in multiple porosities and permeabilities. Worthing (1999) had described of groundwater behavior in carbonate aquifers in terms of triple porosity: intergranular (primary) porosity, fracture porosity, and conduit porosity. Multiple types of porosity in carbonate aquifer resulted in flow behavior that is difficult to characterize, because the porosity and permeability vary throughout the aquifer. The fractures are two-dimensional planar features that occur as bedding planes, joints, or faults. Conduits develop along fractures or other places, where the aquifer is susceptible to solution, and it is believed that these conduits were developed through the shale content or the veins of shale by dissolution and we believe that those conduits are occurred at the aquifer under study because of occurring of shale content. The conduits have the greatest permeability and the least volume of the porosity elements. Where there is faulting, fracture density and the opportunity for conduits to develop through solution processes increase. Both limestone and limy shale are extensively fractured.

High groundwater velocities have physical and chemical impacts on karst aquifer. These velocities allow great volumes of water to move through the aquifer and may dissolve

the aquifer material and enlarge pore spaces. Large volumes of water can be drained directly from the surface into a carbonate aquifer that has solution-enhanced permeability. As a result, when a carbonate aquifer is at the land surface, the landscape has very few surface water features. Water from the surface drains directly into an aquifer through features like sinks and losing streams and may discharge at the surface only at seeps and springs. Drainage occurs within the aquifer, this internal drainage is typical of a karst system and we considered it as pipe lines in the form of fractures and in general taking high curvature lines in the form of vertical and horizontal channels. The most developed parts of the flow system are labeled conduits, which are horizontal and vertical channels that have been altered by the solution of the bed rock.

Ohm’s law stated that the resistance of a conductor is directly proportional to its length and inversely proportional to its cross section. In rocks, it is most often observed that water generally acts as a conductor. The more abundant the water, the wider the cross section of the conductor; the quantity of water depends on porosity and saturation. On the other hand, the length of the conductor is proportionality reduced when the concentrations between pores are direct. From the foregoing, it is clear that the electrical resistivity of a rock essentially depends on its water content, the quality of this water, as well as the nature of its distribution. These factors were taken into account in an extremely important experimental law established for saturated media.

For a rock saturated with water, Archie established an experimental relationship linking the resistivity of the rock, porosity, the nature of distribution, and the resistivity of the electrolyte:

$$\rho_{A/rock(x,y)} = a\rho_w \varphi^{-m} \tag{3}$$

where:  $\rho_{A/rock}$  is the bulk resistivity of the saturated rock (Aquifer) in  $\Omega$  m;  $\rho_w$  is the resistivity of the formation water in  $\Omega$  m;  $\varphi$  is the porosity in %;  $m$  is the cementation factor, fairly constant for a given rock and independent of the fluid, ‘ $m$ ’ characterizes the distance traveled by the electric current; this is the equivalent of what we often call tortuosity. It depends on the shape of the pores and the interconnections between them; it generally varies between 1.3 and 2.2;  $a$  is a factor which depends on the lithology and varies between 0.6 and 2.

In general, the parameters in the above equation characterizing the texture of the rock are known as the formation factor ( $F$ ):

$$F = a \varphi^{-m} . \tag{4}$$

Archie’s expression for a saturated rock then becomes

$$\rho_{rock(x,y)} = F \rho_w . \tag{5}$$

The following relationship is generally accepted for carbonates and formations that are well-cemented and consolidated:

$$F = 1 \varphi^{-2} . \tag{6}$$

Chapellier (1992) reported that the increase in permeability also increases the formation factor. The application of this formula was reported in Table 3, the minimum value of the porosity is 18%, and the maximum value is 25%, while the average value is around 21% for the pure carbonate aquifer. Ammar (2005) estimated the total porosity values of the same formation, Eocene carbonate aquifer, at the Western Desert in Siwa Oasis using the resistivity, density, and neutron logs, and reported that these values were ranged from 7%, when the shale content was high (shaly limestone to limy shale), to 23% in pure fractured limestone and there is no big lowering in effective porosity of the fractured aquifer. From applying the previous equations, it must be taking into account that the effective porosity may be smaller than the calculated total porosity depending upon the type of pore system. Lesmes and Friedman (2005) reported that the porosity of the limestone was ranged from 15 to 29%. All the previous porosity values matched with the calculated values of the porosity of this aquifer. The expected low, high, and average values of porosity are reported in Table 2.

By applying the previous equations and background, the T.D.S., resistivity of water ( $\rho_w$ ), formation factor ( $F$ ), and porosities ( $\varphi\%$ ) are calculated to the saturated carbonate rocks (Table 4). This table and the distribution maps of these parameters show that:

**Table 3** Values of the aquifer resistivity ( $\rho_A$ ), calculated formation factor ( $F$ ) and secondary porosity ( $\varphi$ ) of aquifer and theirs average (above), and expected high, low, and average values of the calculated secondary porosity ( $\varphi$ ) of the aquifer (below)

Wells	$\rho_{A/rock}$ ( $\Omega$ m)	Formation factor ( $F$ )	( $\varphi$ )% Archi’s formula
W8	40	24	20
W9	25	28	18
W10	25	20	22
W11	35	22	21
W12	40	22	21
W13	35	15	25
W14	30	21	21
W15	55	16	24
W16	30	29	18
Average	35	22	21
( $\varphi_{vH}$ )% Very high value	22		
( $\varphi_H$ )% High value	19		
( $\varphi_l$ )% Low value	17		
( $\varphi_{av}$ )% Average value	19		

1. The minimum calculated value of T.D.S. was 674 and the maximum value was 7968 (Fig. 18). On this figure, the areas of high salinity are expected high concentrations in NaCl and CaSO<sub>4</sub>, and high dissolution and low mixed or connected with deep aquifer, while the areas of low salinity are expected low concentration in NaCl and CaSO<sub>4</sub>, and high dissolution, but they are expected more mixed or connected with deep aquifer by faults or mixed with rainwater. The shallow meteoric water may reflect increasing of salinity to pass the rainwater through the fractures and dissolving the different occurring minerals by leaching and it may be low salinity to occur the deep meteoric water that had mixed with the upward water from deep aquifer through the aquifer. On map 18, the maximum values of salinity were detected at the locations of high complicated structurally (faults). We believe that these faults assisted in isolating of these locations which led to increasing in salinity especially to the northeast and south where these faults.
2. The minimum calculated value of the water resistivity ( $\Omega$  m) was 0.8 and the maximum value was 9.5 (Fig. 19). The values of this parameter are more depending on the concentrations of T.D.S. in water, where increasing of water resistivity reflects decreasing of the concentrations of T.D.S. in groundwater and vice versa. On the T.D.S.

map and water resistivity map, the salinity decreases with increasing the resistivity of water as it occurred at the central parts of the area. The minimum and maximum values of the formation factor are 6 and 24, respectively. We believe that the high values of this factor are resulting from high effective porosity which gives indication about high permeability and this confirmed that the assumption of the increase in permeability also increases the formation factor (Chapellier 1992).

3. The minimum and maximum values of the porosities according to Archi's formula are 20 and 39%, respectively, (Fig. 20). The last value may result from the effect of shall content and the expected different types of shall which attendant with the limestone. According to comparison between the formation factor and porosity, it is concluded that the porosity increases with decreasing the formation factor. This result may give indication about increasing of dissolving then fractures then increasing the permeability, because the porosity is factor in formation factor and the permeability is factor in porosity especially the effective porosity.

Most of these parameters as on maps are higher in the areas, where the down-throw than the up-throw of inferred faults and this may reflect and confirm that the

**Table 4** Expected calculated values of the T.D.S., resistivity of water ( $\rho_w$ ), formation factor ( $F$ ), and porosity ( $\phi$ ) of aquifer and theirs averages of the carbonate aquifer

VES no.: 60	$\rho_A$ ( $\Omega$ m)	T.D.S <sub>C</sub> (ppm)	E.C <sub>c</sub> ( $\mu\Omega^{-1}/m$ )	$\rho_{wc}$ in $\Omega$ m	Formation factor	( $\phi$ )% Ar. formula
Min.	11	674	1.1	0.8	6	20
Max.	60	7968	12.5	9.5	24	37
Average	38	3876	6.1	2.8	19	24

**Fig. 18** Measured and calculated of the TDS distribution map of the aquifer

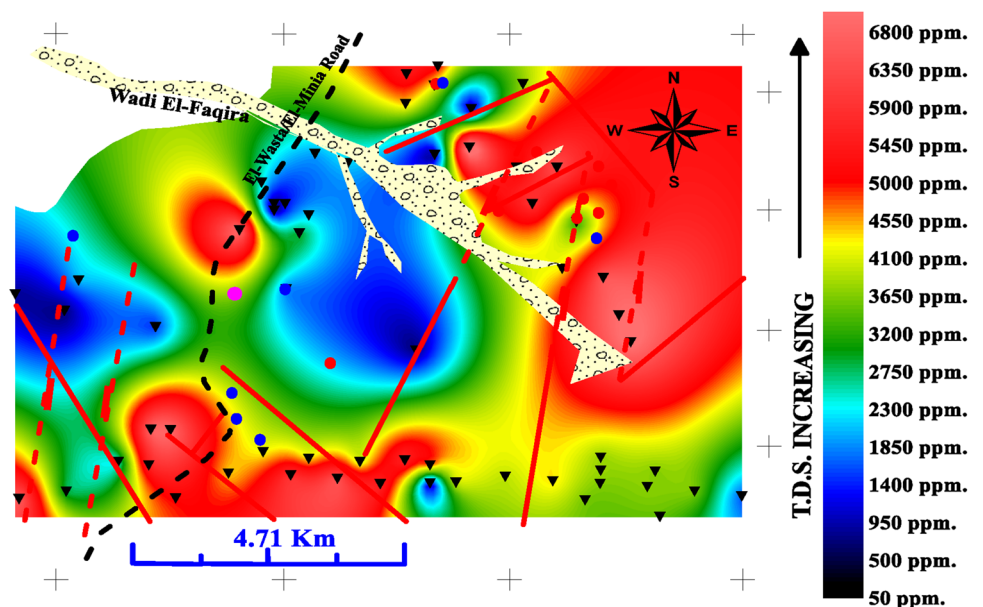


**Fig. 19** Measured and calculated of the water resistivity distribution map of the aquifer

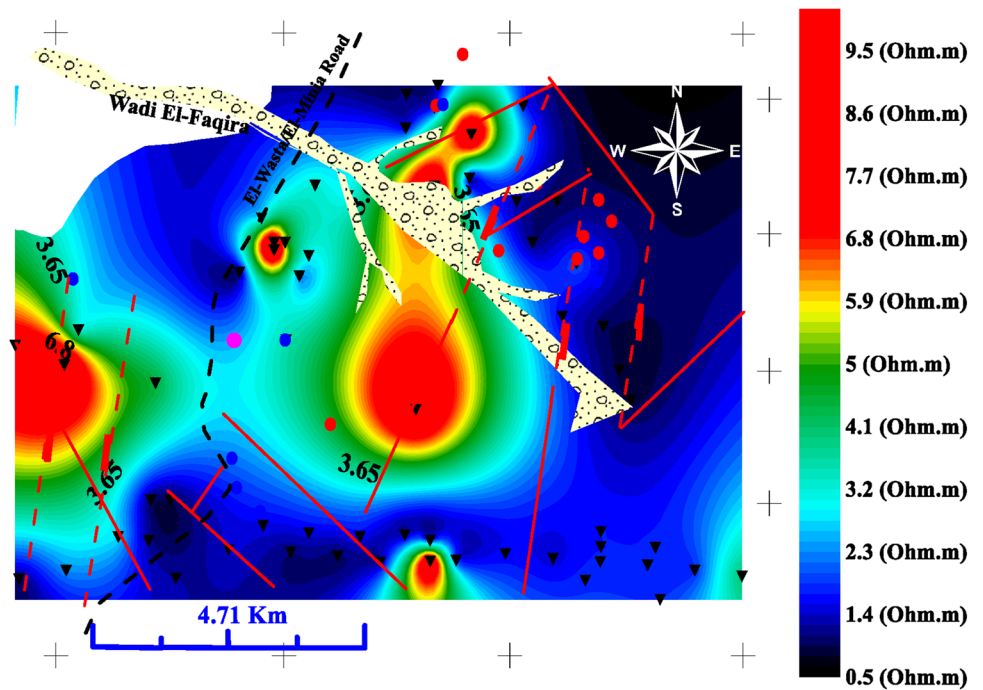
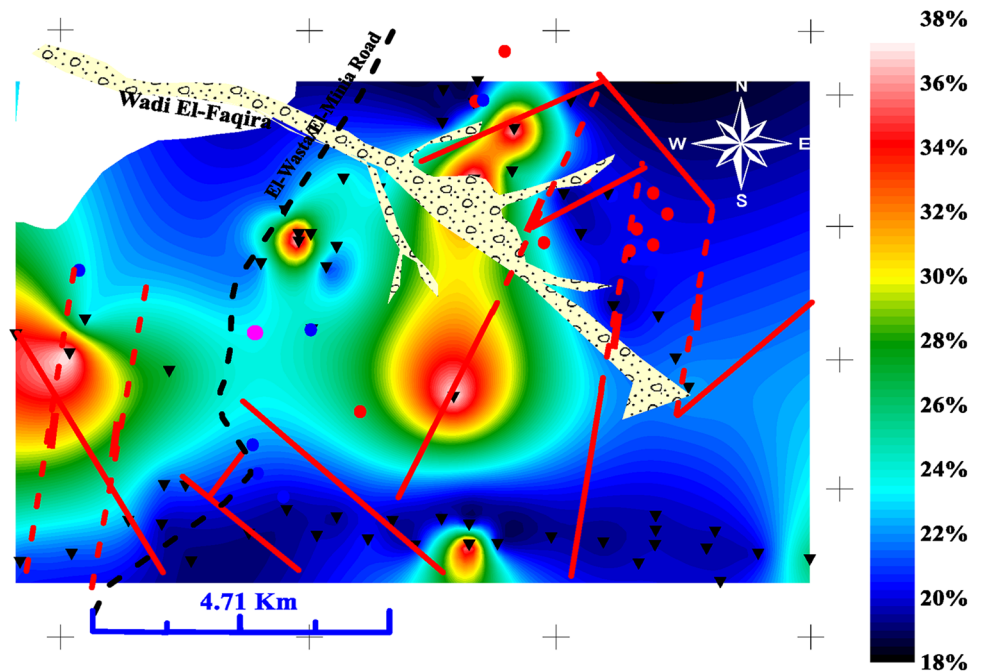


**Fig. 20** Calculated of the porosity distribution map of the aquifer according to Archi's Formula



role of faults in creating and increasing of fractures especially next to it was important and confirming the feeding of aquifer from deep aquifer. In addition, Figs. 21, 22 appear the effect of changing of the water resistivity, electrical conductivity of water, T.D.S., and porosity on changing the bulk resistivity of aquifer.

(E) Hydrochemical analysis significances

In general, the chemical composition of the groundwater aquifer is very important in illustrating its general total dissolved solids (T.D.S.) and its relationship with the anions and cations. This composition reflects the quality of this

**Fig. 21** Effect of changing of the measured water resistivity, electrical conductivity of water, T.D.S., and porosity on changing the calculated bulk resistivity of aquifer at wells

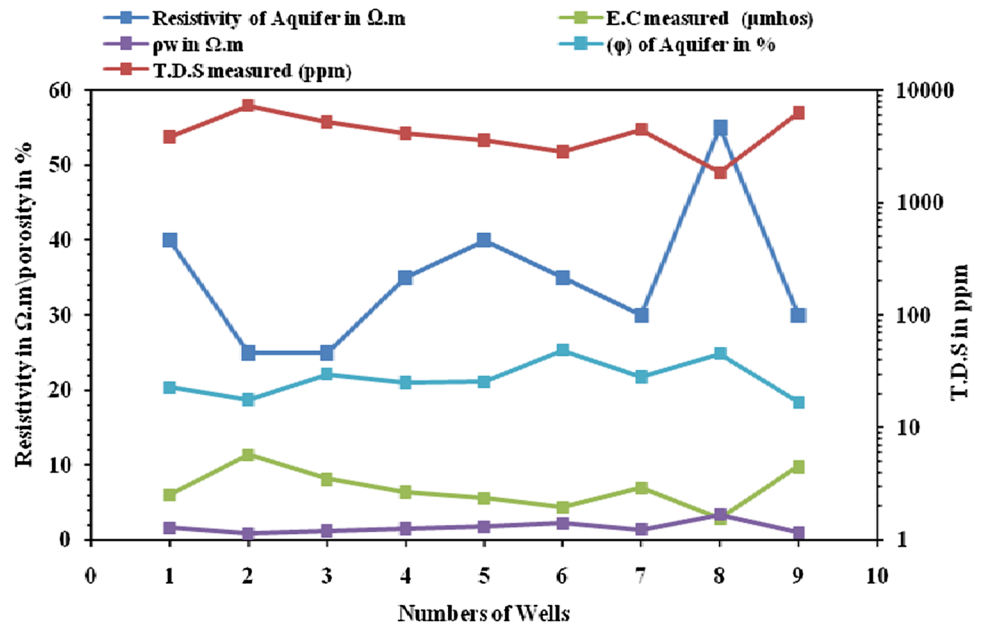
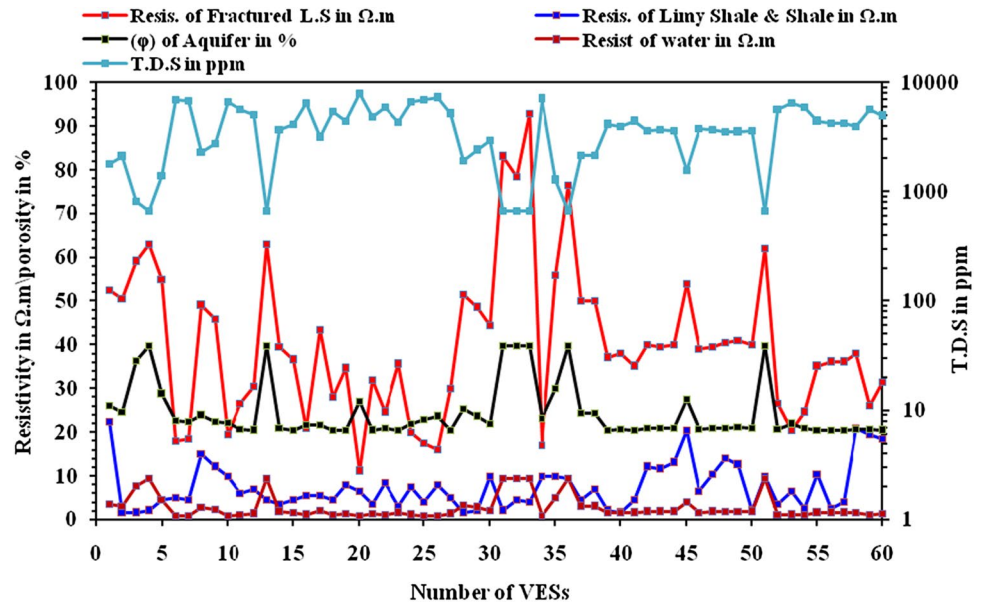


**Fig. 22** Effect of changing of the calculated water resistivity, resistivity of shale, T.D.S., and porosity on changing the calculated bulk resistivity of aquifer at VESs



water and its expected source, recharging and its effect on the conductivity of formation.

1. Major cations included the following:

Na: this cation increases due to seawater or the rock was deposited in marine environmental conditions such as carbonates.

K: this cation decreases, because potassium salts in most rocks is not easily dissolved in groundwater.

Ca: the increasing of Ca content relates to the type of water-bearing strata in which calcite, dolomite, gypsum, and

anhydrite are responsible for enriching the groundwater with calcium ions. In general, the average concentrations of calcium in shale, sandstone, and carbonate rocks are 22,100; 39,100; 30,200 mg/l (ppm), respectively (Turekian and Wedepohl 1961). At this study, the increasing of Ca concentration was expected due to dissolution of limestone rocks.

Mg: the increase of this cation may be resulted from leaching processes of shale that is lagoon and marine in origin adds to more Mg; this will confirm that the occurrence of medium-to-high volumes of shale content in the formation or to mix the leached shale contents from the base of this aquifer.

2. Major anions included the following:

Cl: it is the most common major anions in the natural water and more abundant in seawater.

SO<sub>4</sub>: it increases in groundwater due to dissolution of gypsum minerals included in the water-bearing strata. The relation with Cl was reported weak and indicating local source of sulfate. The sulfate ions reached to groundwater via infiltrate through the top layers then recharge the groundwater system. This will confirm that the source of groundwater is rainwater due to infiltration; the percolating water usually dissolves completely all highly soluble salts such as NaCl, but only partially dissolves sparingly soluble salts such as gypsum (Drever 1982). Therefore, NaCl is more concentration at this aquifer (slightly) than the sulfates.

HCO<sub>3</sub>: it resulted from the slightly dissolution of carbonate rocks.

The results of this analysis (Table 5) are:

- (a) The average value of T.D.S. is 4396 and the highest value is 7276, while the lowest value is 1868.8. These values reflect that the quality of water is brackish.
- (b) The average value of pH is 6.97 and the highest value is 7.2, while the lowest value is 6.27. These values refer that the water of this aquifer is equivalent.
- (c) The concentrations of soluble cations which include Ca<sup>2+</sup>, Mg<sup>2+</sup>, Na<sup>+</sup>, and K<sup>+</sup> range from low to high. Where the Ca<sup>2+</sup> ranges from 60 (low value) to 360.7 (high value) and the average of this cation is around 183. The Mg<sup>2+</sup> ranges from 12 to 194.5 and its average are around 74. The Na<sup>+</sup> ranges from 575 to 1821 and its average is around 1225. While the K<sup>+</sup> ranges from 5 to 12, its average is around 8.5. According to these concentrations, the arrangement of these cations according to their concentrations is Na<sup>+</sup> > Ca<sup>2+</sup> > Mg<sup>2+</sup> > K<sup>+</sup>.
- (d) The concentrations of soluble anions which involved (SO<sub>4</sub>)<sup>2-</sup>, Cl<sup>-</sup>, CO<sub>3</sub><sup>-</sup>, and HCO<sub>3</sub><sup>-</sup> range from low to high. Where the (SO<sub>4</sub>)<sup>2-</sup> ranges from 629 to 1982,

the Cl<sup>-</sup> ranges from 497 to 2662.5, the CO<sub>3</sub><sup>-</sup> characterizes with constant value 30 in all wells, while the HCO<sub>3</sub><sup>-</sup> ranges from 122 to 183 and it may be its value considers stable in all wells. The average values of concentrations of these anions are 1174, 1432, 30, and 129, respectively. From these concentrations, the arrangement of the concentrations of these anions is Cl<sup>-</sup> > (SO<sub>4</sub>)<sup>2-</sup> > HCO<sub>3</sub><sup>-</sup> > CO<sub>3</sub><sup>-</sup>.

- (e) From the relation between the measured T.D.S. of the aquifer and the different major of cations and anions, the most effect on increasing of T.D.S. is Na<sup>+</sup>, Cl<sup>-</sup>, Ca<sup>2+</sup>, Mg<sup>2+</sup>, and then (SO<sub>4</sub>)<sup>2-</sup>, respectively, as shown in Fig. 23. Therefore, the T.D.S. increasing is controlled by increasing of these cations and anions.

All the previous concentration values reflected that the salinity of groundwater is high to low with expecting this salinity may be changed in some locations. The increase of this salinity may be from solubility of the carbonate (calcite and dolomite) according to increase of the carbon dioxide (CO<sub>2</sub>) in water or from solubility of evaporates (gypsum and halite) that interpreted from increasing of sulfate (SO<sub>4</sub>)<sup>2-</sup> with increasing of calcium (Ca<sup>2+</sup>) and increasing of chloride (Cl<sup>-</sup>) with increasing of sodium (Na<sup>+</sup>).

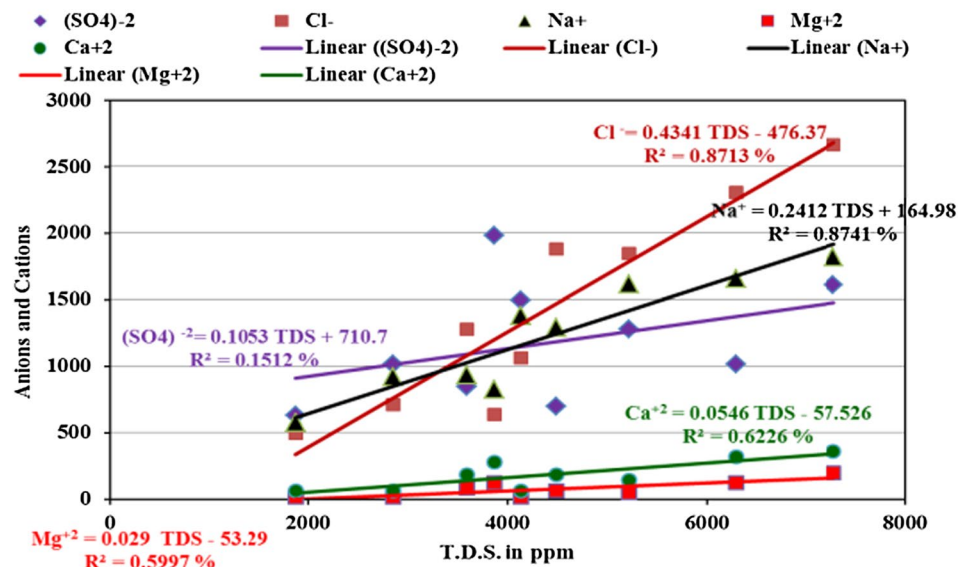
All the previous interpretations may refer to and confirm the source of groundwater from rainwater which may pass through the channels or surface fractures of the upper carbonate layers that rich with evaporates (Beni-Suef Univ., report 2009). It is believed that the main streams or dry wadis such as wadi El-Faqira and its tributaries and other small streams were very interesting streams in feeding and recharging this aquifer. It is expected that there are several chemical reactions that were burnet during soluble evaporates and some carbonates and add to the tectonic setting, where those tectonics assisted in feeding of this aquifer from the low saline water of the deep sandstone aquifer.

It is believed that the shale content at the shaly limestone and the shale layer evaporates into shales that are considered the main source of salinity. In addition, it is believed that

**Table 5** Chemical analysis to groundwater samples of the carbonate aquifer (after Faculty of Science, Beni-Suef University 2009)

Wells	T.D.S <sub>m</sub> (ppm)	(SO <sub>4</sub> ) <sup>2-</sup>	CL <sup>-</sup>	CO <sub>3</sub> <sup>-</sup>	HCO <sub>3</sub> <sup>-</sup>	K <sup>+</sup>	Na <sup>+</sup>	Mg <sup>2+</sup>	Ca <sup>2+</sup>	pH
W8	3865.5	1982.5	639	30	122	11.5	827.5	121.5	280.5	7.14
W9	7277	1608	2662.5	30	122	10.5	1821	194.5	361	7.03
W10	5216	1277	1846	–	183	8.5	1618.5	48.5	140	6.9
W11	4128	1498	1065	30	122	7	1379.5	12	60	7.2
W12	3584	845	1278	30	122	7	931	85	180.5	7.08
W13	2848	1018	710	30	122	6.5	919.5	12	60	7.04
W14	4486	696	1881.5	30	122	9.5	1294	61	180.5	7.05
W15	1869	629	497	–	122	5	575	12	60	7.04
W16	6291	1012	2307.5	–	122	12	1660	121.5	321	6.27
Average	4396.1	1173.8	1431.8	30	128.8	8.5	1225.1	74.3	182.6	6.97

**Fig. 23** Relation between T.D.S.m of the aquifer and its depending on the major cations and anions



the salinity may increase with increasing the discharge from eastern area and decreased at the western areas especially at the closed areas to the Nile valley, where their feeding may expect from the Nile River especially at the downstream of wadis. All the previous results require other several studies for confirmation.

### 3. Sulin's classification

Skinner and Porter (1987) had reported that the silicates are most abundant minerals on the earth, a number of others—principally oxides, sulfides, carbonates, phosphates, and sulfates are common enough to be called rock-forming minerals. The complex carbonate anion ( $\text{CO}_3^-$ ) forms three important and common minerals: calcite, aragonite, and dolomite. They had already seen that calcite and aragonite have the same composition,  $\text{CaCO}_3^-$ , and are polymorphs. Calcite is much more common than aragonite. Dolomite has the formula  $\text{CaMg}(\text{CO}_3)_2$ . In addition, they had reported that sulfate minerals contain the complex anion  $(\text{SO}_4)^{2-}$ . Although many sulfates are known, only two are common, and both are calcium sulfate minerals: anhydrite,  $\text{CaSO}_4$ ; and gypsum,  $\text{CaSO}_4 \cdot 2\text{H}_2\text{O}$ , both form when seawater evaporates, carbonates (calcite, aragonite, and dolomite), and sulfates (anhydrite and gypsum).

Sulin's graph (1946) (Fig. 24) for genetic classification of groundwater was used to indicate the water genesis and water type using the hydrochemical composition (Table 6). Groundwater has been divided into four genetic types:

(f) Sulfate–sodium type of meteoric water in origin and associated sulfates is derived from terrestrial conditions.

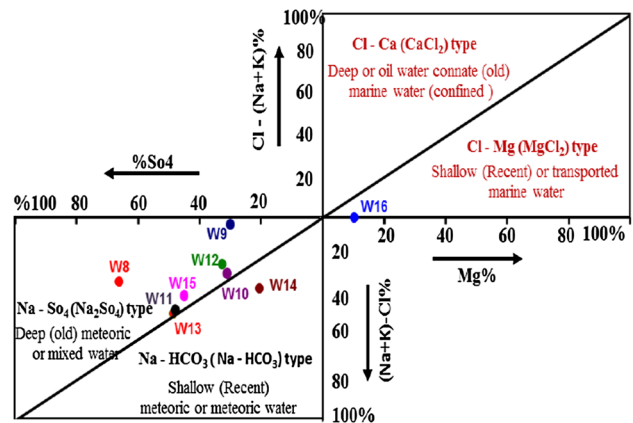


**Fig. 24** Sulin's graph for genetic classification of the groundwater of the carbonate aquifer

- (g) Bicarbonate–sodium type in which water reflects meteoric associations and continental conditions for the bicarbonates.
- (h) Chloride–magnesium type in which water reflects marine environment and evaporates sequences.
- (i) Chloride–calcium type that is associated with subsurface water bodies that could be non-meteoric.

According to Sulin's classification, most of the samples located in the lower quadrant of Sulin's diagram (Fig. 24) and characterized by sodium–bicarbonate and sodium–sulfate genetic water types, indicating meteoric water in origin. The hydrochemical composition of the different studied water samples was interpreted to determine the water genesis and the formation of chemical composition at different environment. Therefore, the majority of the studied



**Table 6** Expected water type and origin/geneses of groundwater of the carbonate aquifer

Wells	(K + Na)-Cl (%)	SO <sub>4</sub> (%)	Water type	Water origin/geneses from Sulin's classification
W8	33.5	66	Na, SO <sub>4</sub> , Cl, Ca, and Mg = (Na-SO <sub>4</sub> )	Deep (old) meteoric/mixed water
W9	3	30	Na, Cl, SO <sub>4</sub> , Ca, and Mg = (Na-Cl)	Deep (old) meteoric/mixed water
W10	23	32.5	Na, Cl, and SO <sub>4</sub> = (Na-Cl)	Deep (old) meteoric/mixed water
W11	47	48.5	Na, SO <sub>4</sub> , and Cl, = (Na-SO <sub>4</sub> )	Deep (old) meteoric/mixed water
W12	27	31	Na, Cl, and SO <sub>4</sub> = (Na-Cl)	Deep (old) meteoric/mixed water
W13	45.5	48	Na, SO <sub>4</sub> , and Cl = (Na-SO <sub>4</sub> )	Shallow (recent) meteoric water
W14	35	20.5	Na, Cl, and SO <sub>4</sub> = (Na-Cl)	Shallow (recent) meteoric water
W15	38	45	Na, Cl, and SO <sub>4</sub> = (Na-Cl)	Deep (old) meteoric/mixed water
W16	0.2	10	Cl, Na, SO <sub>4</sub> , and Ca (Na-Cl)	Shallow (recent) marine/mixed water

water samples were fell within the triangles of the Na<sub>2</sub>SO<sub>4</sub> representing meteoric origin. There was one sample fell in NaHCO<sub>3</sub> and the other one fell in MgCl<sub>2</sub>.

The Na<sub>2</sub>SO<sub>4</sub> water type reflects deeply percolated meteoric water which is believed upward through the faults from the deep sandstone aquifer. The last aquifer was overlaid by shale and shaly rocks then the carbonate rocks at the eastern and western desert (Ammar 2005). This gives rise to the gradual increase in the concentration of sulfate ions due to leach of sulfate minerals from rock constituents. The sample was fell in NaHCO<sub>3</sub> water type, revealed meteoric water genesis of shallow water conditions due to the reduction of the sulfate ions by anaerobic bacteria, and in the presence of carbon content, they give the bicarbonate ions. The sample fell within the triangle of MgCl<sub>2</sub> water type and it may be under affected intermixing between the fresh water and saline water.

## Conclusion

Sixty VESs were carried out as well as 17 productive wells for studying the structural and hydro-geophysical settings of the carbonate aquifer. The general recorded curve type was QKH. These curves were used in delineating of the zones of faults depending on their intersecting and the depth of this intersecting between each two curves next to each other. Accordingly, it was found congruence between the mapped faults using geological data and the delineated faults using the geoelectrical data. These VESs were interpreted and concluded that there are seven geoelectrical layers. The saturated fractured limestone and shaly limestone were considered the main water-bearing layer and their resistivities values changed from low to medium (11–93 Ω m). Those values assisted in delineating the expected locations of very high, high, and intermediate fractures density, groundwater accumulations and its expected quality and quantity. From the

statistical analyses, the resistivity of aquifer decreases with increasing the T.D.S. and increases with increasing the water resistivity and these variables differ significantly for different each other. The two resulted formulas can be used in estimating the T.D.S. and water resistivity from the aquifer resistivity. We should mention that the calculated aquifer parameters are well-defined within the range of observed aquifer parameters. The T.D.S. increasing is controlled by Na<sup>+</sup>, Cl<sup>-</sup>, Ca<sup>2+</sup>, Mg<sup>2+</sup>, and then (SO<sub>4</sub>)<sup>2-</sup>, respectively. The average calculated porosity of the aquifer was 19%. From the hydrochemical analyses, the water type was brackish, the arrangements of cations concentrations were Na<sup>+</sup> > Ca<sup>2+</sup> > Mg<sup>2+</sup> > K<sup>+</sup>, while anion concentrations were Cl<sup>-</sup> > (SO<sub>4</sub>)<sup>2-</sup> > HCO<sub>3</sub><sup>-</sup> > CO<sub>3</sub><sup>-</sup>, and the salinity was high to low. The source of groundwater was from rainwater. Most of the samples were characterized by sodium–bicarbonate and sodium–sulfate genetic water types and indicated meteoric water in origin. The majority of these samples were represented deeply percolated meteoric origin from deep sandstone aquifer, while one sample was revealed meteoric water genesis of shallow water conditions and the other one may be under affected intermixing between the fresh water and saline water. At the end, the DC-resistivity method can be used in delineating of the zones of faults and assisted in understanding and determining the hydro-geophysical characteristics of the fractured carbonate aquifer.

**Acknowledgements** Research Institute for Groundwater, National Water Research Center, Egypt is appreciated with its assistance us in acquiring the geological, hydrogeological data, and field geoelectric measurements. In addition, it assisted and allowed in confirming the outputs by field trips and following up these outputs. We appreciate valuable comments from reviewers as well as the assisting from the editor-in-chief, Prof. Dr. Saad A. Al-Jilil in fast reviewing of this paper.

**Open Access** This article is distributed under the terms of the Creative Commons Attribution 4.0 International License (<http://creativecommons.org/licenses/by/4.0/>), which permits unrestricted use, distribution, and reproduction in any medium, provided you give appropriate credit

to the original author(s) and the source, provide a link to the Creative Commons license, and indicate if changes were made.

## References

- Abd El-Mageed GM (2002) Hydrogeological and environmental impacts of agricultural efforts in Beni-Suef area, Nile valley, Egypt. Ph.D. Thesis, Faculty of Science, Ain Shams Univ
- Ammar AI (2005) The contribution of surface and subsurface geophysical investigations in solving the over-pressuring problem of the groundwater in Siwa area, Egypt. Ph.D. Thesis, Faculty of Science, El-Zagazig Univ
- Ammar AI (2013) Fractures density mapping using DC resistivity and its effects on water accumulation in Tir'ah and Ad Dar'ah Areas, Wadi Al'ays Quadrangle, Saudi Arabia. 5 International conference on water resources and arid environments (ICWRAE 5), Riyadh, Saudi Arabia, pp 121–133
- Ammar AI, Monem M (2011) Simulating the expected flow direction of groundwater in Wadi El-Natron Area, Western Desert, Egypt, using the resistivity method. *J Appl Geophys* 10(1):205–219
- Atre SR, Carpenter PJ (2010) Identification of cross-valley faults in the Maynardville Limestone, Oak Ridge Reservation, Tennessee, using seismic refraction tomography. *Environ Earth Sci* 60:1245–1256. <https://doi.org/10.1007/s12665-009-0265-4>
- Bauer H, Schröckenfuchs TC, Decker K (2016) Hydrogeological properties of fault zones in a karstified carbonate aquifer (Northern Calcareous Alps, Austria). *Hydrogeol J* 24:1147–1170. <https://doi.org/10.1007/s10040-016-1388-9>
- Cemen I, Young R, Halihan T (2008) Determination of fracture density in the Arbuckle-Simpson aquifer from ground penetrating radar (GPR) and resistivity data. Final technical report, Oklahoma Water Resources Research Institute
- Chandra S, Rao VA, Krishnamurthy NS, Dutta S, Ahmed S (2006) Integrated studies for characterization of lineaments to locate groundwater potential zones in hard rock region of Karnataka, India. *Hydrogeol J* 14(5):767–776
- Chapellier D (1992) Well logging in hydrogeology. *Trans., of: Diagraphies Appliqués a L'hydrologie. A.A., Balkema/Rotterdam/Brookfield*. ISBN 9054102071
- Drever JJ (1982) The geochemistry of natural water. *Soil Sci* 69:123–134
- Faculty of Science, Beni-Suef Univ. (2009) Geological and hydrogeological studies on groundwater aquifer in Beba and El-Fashn towns (Wadi El-Faqira and Wadi El-Madle), East of Nile River, Beni-Suef governorate, Egypt
- Ford DC, Williams P (2007) *Karst hydrogeology and geomorphology*. Wiley, Chichester
- Frohlich RK, Williams JB, Boland MP (1988) A geological study of hydraulic bedrock conditions in Aroostook County, Maine. In: *Proceedings of the symposium of the international conference on fluid flow in fractured rocks, held in Atlanta, May 1988*, pp 114–124
- Frohlich RK, Fisher JJ, Summerly E (1996) Electric–hydraulic conductivity correlation in fractured crystalline bedrock: central Landfill, Rhode Island, USA. *J Appl Geophys* 35:249–259
- Ganerød GV, Rønning JS, Dalsegg E, Elvebakk H, Holmøy K, Nilsen B, Braathen A (2006) Comparison of geophysical methods for sub-surface mapping of faults and fracture zones in a section of the Viggja road tunnel, Norway. *Bull Eng Geol Environ* 65:231–243. <https://doi.org/10.1007/s10064-006-0041-6>
- Halihan T (2008) Evaluating groundwater–surface water interactions using ERI in the Arbuckle-Simpson aquifer. GSA South-Central Sectional Meeting, Hot Springs, AK, April 2008. In: *Geological Society of America abstracts with programs, vol 40, Issue 3*
- Herwanger JV, Worthington MH, Lubbe R, Binley A (2004) A comparison of cross-hole electrical and seismic data in fractured rock. *Geophys Prospect* 52:109–121
- Kazemi R, Porhemmat J, Kheirikhah M (2009) Investigation of lineaments related to groundwater occurrence in a karstic area, A case study in Iar catchment, Iran. *Res J Environ Sci* 3:367–375. <https://doi.org/10.3923/rjes.2009.367.375>. <http://Scialert.net/abstract/?doi=rjes,2009.367.375>
- Khaled MA, Al Tammamy AM, Barseem MS, El Sayed AN, El Abed EA (2016) Geoelectrical and hydrogeological study to delineate the geological structures affecting the groundwater occurrence in Wadi El Khariq Basin, Northwest El Maghara, north Sinai, Egypt. *Arab J Geosci* 9:271. <https://doi.org/10.1007/s12517-015-2286-5>
- Lattman LH, Parizek RR (1964) Relationship between fracture traces and the occurrence of groundwater in carbonate rocks. *J Hydrol* 2(2):73–91. [https://doi.org/10.1016/0022-1694\(64\)90019-8](https://doi.org/10.1016/0022-1694(64)90019-8)
- Lesmes DP, Friedman SP (2005) Relationships between the electrical and hydrogeological properties of rocks and soils. In: Rubin Y, Hubbard SS (eds) *Hydrogeophysics. Water science and technology library, vol 50*. Springer, Dordrecht. [https://doi.org/10.1007/1-4020-3102-5\\_4](https://doi.org/10.1007/1-4020-3102-5_4)
- Meir NV, Jaeggi D, Herfort M, Loew S, Pezard PA, Lods G (2007) Characterizing flow zones in a fractured and karstified limestone aquifer through integrated interpretation of geophysical and hydraulic data. *Hydrogeol J* 15:225–240. <https://doi.org/10.1007/s10040-006-0086-4>
- MINITAB (1998) *Statistical software package. Licensed to analysis of the statistical environmental data*
- Nelson RA (2001) *Geological analysis of naturally fractured reservoir, 2nd edn*. Elsevier, Amsterdam, pp 125–161. ISBN 978-0-88415-317-7
- Niwas S, de Lima OAL (2003) Aquifer parameter estimation from surface resistivity data. *Ground Water* 41:94–99
- Pánek T, Margielewski W, Táborík P, Urban J, Hradecký J, Szura C (2010) Gravitationally induced caves and other discontinuities detected by 2D electrical resistivity tomography: case studies from the Polish Flysch Carpathians. *Geomorphology* 123:165–180
- Parizek RR (1976) Lineaments and groundwater. In: McMurty GT, Petersen GW (eds) *Interdisciplinary applications and interpretations of EREP (Skylab) data within the Susquehanna River Basin*. Skylab EREP Investing. #475 NASA Contrib. Penn State Univ., pp 4–59 to 4–86
- Purvanca DT, Andricevic R (2000a) Geoelectric characterization of the hydraulic conductivity field and its spatial structure at variable scales. *Water Resour Res* 36:2915–2924
- Purvanca DT, Andricevic R (2000b) On the electrical–hydraulic conductivity correlation in aquifers. *Water Resour Res* 36:2905–2913
- Redhaounia B, Ilondo BO, Gabtni H, Sami K, Bédir M (2016) Electrical resistivity tomography (ERT) applied to Karst carbonate aquifers: case study from Amdoun, Northwestern Tunisia. *Pure Appl Geophys* 173:1289–1303. <https://doi.org/10.1007/s0024-015-1173-z>
- Rinvert (1999) *Geophysical software package: licensed to hydrogeology and engineering geology. Hochi Minh City-Vietnam., Reg., Number, RW 140032, February 03, 1999*
- Robert T, Dassargues A, Brouyère S, Kaufmann O, Hallet V, Nguyen F (2011) Assessing the contribution of electrical resistivity tomography (ERT) and self-potential (SP) methods for a water well drilling program in fractured/karstified limestones. *J Appl Geophys* 75:42–53. <https://doi.org/10.1016/j.jappgeo.2011.06.008>
- Serra O (1984) *Fundamental of well-log interpretation: the acquisition of logging data, developments in petroleum science, vol 1. 15A-trans., El Sevier Science Publishers B.V., Amsterdam, The Netherlands*

- Sharma PV (1997) Environmental and engineering geophysics. Cambridge University Press, Cambridge. <https://doi.org/10.1017/CBO9781139171168.002>
- Shipton Z, Soden A, Kirkpatrick J et al (2006) How thick is a fault? Fault displacement-thickness scaling revisited. In: Abercrombie R, McGarr A, Toro GD et al (eds) Earthquakes: radiated energy and the physics of faulting, vol 170. AGU monograph series. AGU, Washington, DC, pp 193–198
- Siddiqui SH, Parizek RR (1971) Hydrogeologic factors influencing well yields in folded and faulted carbonate rocks in Central Pennsylvania. *Water Resour Res* 7:1295–1312
- Skinner BJ, Porter SC (1987) Physical geology. Wiley, USA. ISBN 0-471-05-668-5
- Solomon S, Ghebream W (2008) Hard-rock hydrotectonics using geographic information system in the central high lands of Eritrea: implications for groundwater exploration. *J Hydrol* 349(1–2):147–155. <https://doi.org/10.1016/j.jhydrol.2007.10.032>
- Sulin VA (1946) Water of petroleum formation in the system of nature water. Gostop Tkhizdat, Moscow, Russia (**in Russian**)
- Turekian KK, Wedepohl KH (1961) Distribution of the elements in some major units of the Earth's crust. *Bull Geol Soc Am* 72(2):175–192
- Worthing SRH (1999) A comprehensive strategy for understanding flow in carbonate aquifer. In: Palmer AN, Palmer MV, Sasowsky ID (eds) Karst modeling, karst waters institute special publication 5. Proceedings of the symposium, February 24–27, 1999, Charlottesville, VA: Charles Town, W.Va., Karst Waters Institute
- Zhu J, Currens JC, Dinger JS (2011) Challenges of using electrical resistivity method to locate karst conduits—a field case in the Inner Bluegrass Region, Kentucky. *J Appl Geophys* 75:523–530. <https://doi.org/10.1016/j.jappgeo.2011.08.009>
- Zohdy AR, Bisdorf RJ (1989) Schlumberger sounding data processing and interpretation program. U.S., Geological Survey, Denver, Co

**Publisher's Note** Springer Nature remains neutral with regard to jurisdictional claims in published maps and institutional affiliations.